Journal of Geosciences, 57 (2011), 273–298 DOI: 10.3190/jgeosci.098

Original paper

Mineralogy and origin of supergene mineralization at the Farbište ore occurrence near Poniky, central Slovakia

Martin ŠTEVKO[1*], Jiří SEJKORA[2], Peter BAČÍK[1]

[1] *Department of Mineralogy and Petrology, Faculty of Natural Sciences, Comenius University, Mlynská dolina G, 842 15 Bratislava, Slovak Republic; stevko@fns.uniba.sk*

[2] *Department of Mineralogy and Petrology, National Museum, Václavské nám. 68, 115 79 Prague 1, Czech Republic*

[*] *Corresponding author*

Supergene mineralization at the hydrothermal Farbište ore occurrence near Poniky, central Slovakia, was studied using optical and electron scanning microscopy, X-ray powder diffraction, electron microprobe and IR spectroscopy. Two principal associations of the supergene minerals were observed. The first is represented mostly by tyrolite with a higher content of sulphate groups and chrysocolla associated with copper carbonates. The second is characterized by a rich assemblage of copper arsenates: low-S tyrolite, strashimirite, parnauite, olivenite, cornwallite, cornubite, euchroite and clinoclase, which occur together with chrysocolla, bariopharmacosiderite-Q, brochantite, azurite and malachite. Both associations formed as a result of decomposition of primary ore minerals, especially tennantite, which is the prevalent primary ore mineral at the Farbište occurrence and was the main source of Cu, As and S ions in the supergene zone.

Keywords: supergene mineralization, copper minerals, arsenates, Farbište near Poniky, Slovakia
Received: 20 December 2010; accepted: 25 August 2011; handling editor: J. Plášil

1. Introduction

Study of supergene mineral associations and minerals present in oxidation zones of sulphide ore deposits/occurrences may lead to a better understanding of the geochemical behaviour of elements such as Cu, Pb and As in near-surface parts of the Earth's crust. Supergene minerals and their stability play a key role in mobility of these elements. Study of these minerals elucidates mechanism of element transportation and accumulation under the natural conditions (Magalhães et al. 1986, 1988; Williams 1990; Krivovichev et al. 2006).

The occurrence of supergene minerals at Farbište, Central Slovakia, has been known in the literature for more than a century, but general data for supergene phases are lacking. Zipser (1817) described an occurrence of azurite, chrysocolla, malachite and pseudomalachite, while tyrolite was first mentioned by Zepharovich (1859). Láznička (1965) reported also euchroite and erythrite, while clinoclase, strashimirite and olivenite were identified by Řídkošil (1981a). A short note on the presence of cornwallite and cornubite was published by Hyršl et al. (1984). Recently, a report on new finds of supergene minerals from Farbište was given by Števko et al. (2010).

This paper presents data obtained by detailed study of newly collected samples with particular focus on chemical composition and associations of supergene minerals at this locality, which is particularly rich in rare copper arsenates like euchroite, strashimirite and parnauite and represents a suitable model object for study of copper and arsenic behaviour under supergene zone conditions.

2. Geological setting

2.1. Regional geology

The small abandoned Cu deposit Farbište is situated on the southern slopes of the Farbište Hill (675 m a.s.l.), *c.* 4 km NE of Poniky village (Fig. 1) in the Ponická vrchovina Mts., Slovak Republic. The Poniky and Bystrica highlands constitute part of a larger geographic entity – the Zvolen Basin (Mazúr and Lukniš 1980). Several geological units participate in the rather complicated Palaeo-Alpine structure of the region, including Veporic, Fatric, Hronic and Silicic units, sediments of Palaeogene age and accumulations of Neogene volcanics (Fig. 1). The *Veporic Unit* consists of a crystalline complex, Late Palaeozoic clastic sediments of the Ľubietová Group, and the Veľký Bok envelope sequence of the Mesozoic age. Migmatized paragneisses, banded migmatites and granite porphyries are the dominant crystalline rocks in the Poniky area (Polák et al. 2003b). In the Suchá Driekyňa Valley occur Late Palaeozoic clastic sediments of the Ľubietová Group (Vozárová and Vozár 1988). The Mesozoic Veľký Bok envelope sequence and lithologically closely similar *Fatric Unit* include sediments of Triassic to Cretaceous age (Polák et al. 2003b). The *Hronic Unit* is represented mainly by complex of Me-

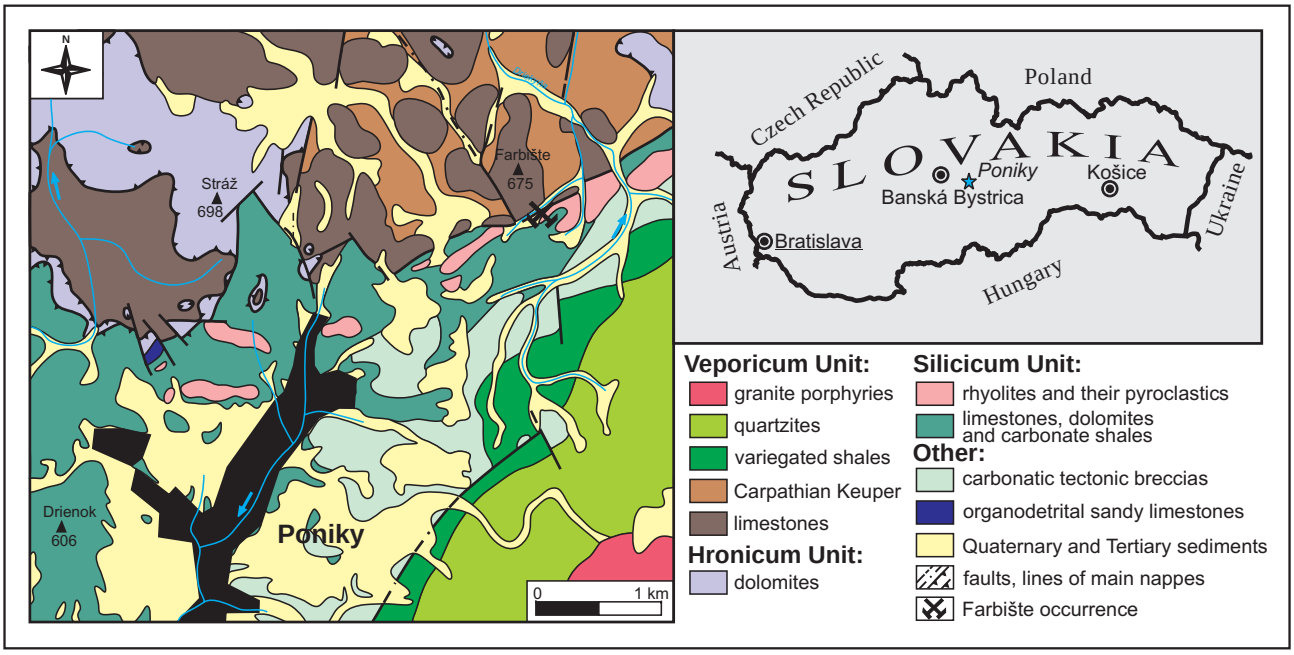

Fig. 1 Generalized geological map showing the location of Farbište ore occurrence near Poniky (Polák et al. 2003a, modified).

sozoic sedimentary rocks. The clastic sediments and tholeiitic volcanic rocks of the Hronic Unit (Ipoltica Group) occur only north of Poniky in the Slovenská Ľupča (Vozárová and Vozár 1988). The Mesozoic rocks in the Hronic Unit are mainly Triassic limestones and dolomites. The *Silicic Unit* in the Poniky area (Drienok Nappe, Bystrický 1964) has a stratigraphic range from Lower to Upper Triassic (Polák et al. 2003b). A characteristic Lower Triassic member of the Drienok Nappe are acid volcanites and associated pyroclastic rocks (Slavkay 1965). Middle and Upper Triassic is developed as limestones and dolomites (Polák et al. 2003b).

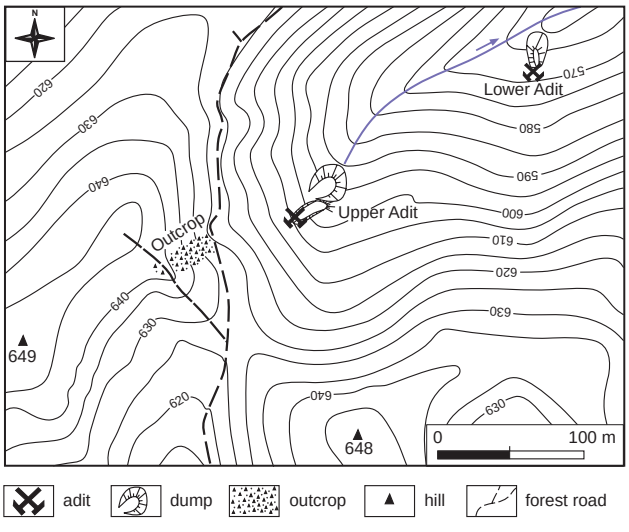

Fig. 2 Schematic topographic map of the Farbište occurrence showing the mining objects and outcrop location.

2.2. Copper mineralization of the Farbiště occurence

Early exploration and small-scale mining at the locality took place in the 19th century in an adit situated in the supergene zone (Figs 2, 3a). In 1959–1960, an extensive geological exploration (boreholes, test pits) was started. The 19th century adit was re-opened and primary mineralization in the deeper parts of deposit explored via a new adit (Losert 1965; Slavkay et al. 1968). This research confirmed that the mineralization is non-economic and estimated reserves of copper are small (Slavkay et al. 1968; Slavkay 1971).

Hydrothermal copper mineralization at the Farbište occurrence has characteristics of a stockwork–impregnation zone with NE–SW strike, dip 30–60° to SE and maximum thickness of 10 m (Losert 1965; Slavkay 1971). The ore mineralization is hosted in Lower Triassic rhyolites, andesites and their pyroclastic derivates belonging to the Silicic Unit (Slavkay 1965; Slavkay et al. 1968) (Fig. 1). According to Uher et al. (2002a), the rhyolites are potassium-rich and of anorogenic nature, with porphyric texture. All these volcanic rocks are interpreted as indicators of early Alpine continental rifting (Putiš et al. 2000).

The primary ore mineralization at Farbište is rather simple. The main ore mineral is tennantite accompanied by pyrite, bornite, chalcopyrite, chalcocite and hematite (Kravjanský 1962; Losert 1965; Slavkay 1971). Kotásek and Kudělásek (1962) identified galena as microscopic corroded grains in limonite. Láznička (1965) mentioned also covellite. Gangue minerals are represented by quartz and baryte (Slavkay 1971). Kravjanský (1962) identified

Fig. 3a – Dump of upper adit at the Farbište occurrence. Situation in May 2008. **b –** Outcrop with supergene mineralization. Situation in October 2009. Both photos by B. Bureš.

the following succession scheme of the primary minerals: quartz → pyrite → bornite → chalcopyrite → tennantite → chalcocite → barite. The supergene zone extends to depths of 50 m. It is well exposed on outcrop (Fig. 3b) and in erosion rills situated above the upper adit.

3. Experimental techniques

3.1. Morphological study

The surface morphology of samples was studied using an Olympus SZ61 optical microscope in combination with an Olympus SP-350 digital camera and QuickPHOTO MICRO 2.2 software (Martin Števko, Department of Mineralogy and Petrology, Faculty of Natural Sciences, Comenius University, Bratislava) or with a Leitz Ortholux I optical microscope in combination with a Canon EOS 400 D digital camera (Volker Betz), used for photography in incandescent light. Depth of focus of photos was reached by layering composition of a number of pictures using the Deep Focus 3.1 (Martin Števko) or Helicon Focus software (Volker Betz).

Details of surface morphology of gold-coated samples were studied using a Jeol Superprobe JXA-840A scanning electron microscope (SEM) under the following conditions: accelerating voltage 15 kV and specimen current 6 nA (Faculty of Natural Sciences, Comenius University, Bratislava).

3.2. X-ray powder diffraction study

Step-scanned powder diffraction data were collected using a Bruker D8 Advance diffractometer (Laboratory of X-ray diffraction SOLIPHA, Faculty of Natural Sciences, Comenius University, Bratislava) under following conditions: Bragg-Brentano geometry (θ–2θ), Cu anode, Lynx-Eye detector, accelerating voltage 40 kV, beam current 40 nA, step size 0.01° 2θ and the step time 3 s. NiK_β filter was used for stripping of K_β radiation on the primary beam. The studied samples were placed on the surface of a flat silicon wafer from suspension in ethanol. The results were processed using the X-ray analysis software Bruker DIFFRAC^{plus} EVA, and unit-cell parameters were refined with the Bruker DIFFRAC^{plus} TOPAS program using Rietveld refinement mode.

3.3. Chemical analyses

Quantitative chemical data were collected using Cameca SX100 electron microprobe (Laboratory of Electron Microscopy and Microanalysis of the Masaryk University and Czech Geological Survey, Brno) operating in the wavelength-dispersion mode with an accelerating voltage of 15 kV, a specimen current of 8–10 nA, and a beam diameter of 5–10 μm. The following X-ray lines and standards were used: K_α: andradite (Ca, Fe), albite (Na), barite (S), sanidine (Al, Si, K), fluorapatite (P), ZnO (Zn), olivine (Mg), rhodonite (Mn), vanadinite (V), topaz (F), halite (Cl); L_α: InAs (As), dioptase (Cu), Sb (Sb); M_α: vanadinite (Pb) and M_β: Bi (Bi). Peak counting times were 20 s for main elements and 60 s for minor elements; each background was counted for a half of peak time. Raw intensities were converted to concentrations using the automatic *PAP* (Pouchou and Pichoir 1985) matrix correction software package. Elevated analytical totals for minerals containing a large amount of hydroxyl groups or crystal water are generally caused by water evaporation under high-vacuum conditions or its evaporation due to heating of the analyzed spot by the electron beam. Lower analytical totals for some samples are primarily due to their

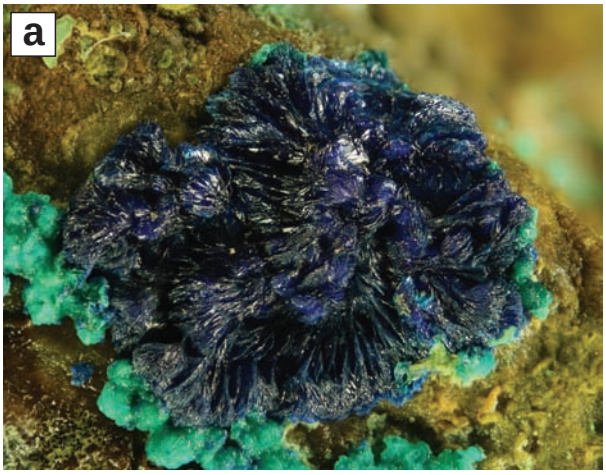

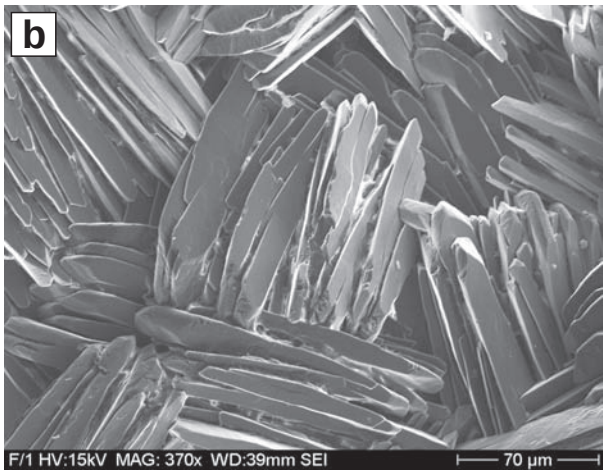

Fig. 4a – Radial aggregate of azurite crystals associated with irregular to hemispherical aggregates of euchroite. Width of area is 8 mm. Photo V. Betz. **b –** Parallel oriented thick tabular crystals of azurite; SEM photo by M. Števko.

porous nature or poorly polished surfaces of soft or cryptocrystalline minerals.

3.4. Infrared spectroscopy

Mid infrared spectra (4000–400 cm^{-1}) were recorded by micro diffuse reflectance method (DRIFTS) using a Nicolet 6700 FTIR spectrometer with DTSG detector (Institute of Inorganic Chemistry, Slovak Academy of Sciences, Bratislava). Each handpicked monomineralic sample was mixed with KBr (1 mg of sample to 200 mg of KBr). Obtained data were processed using the OMNIC 8.1. software (Nicolet Instruments Corp.).

4. Description of minerals and their properties

4.1. Carbonates

4.1.1. Azurite

Azurite is one of the most common supergene minerals, together with malachite. It usually occurs as pale to bright-blue coatings, crystalline crusts and impregnations on fissures of mineralized rocks. Well developed, dark-blue prismatic azurite crystals up to 2 mm long with vitreous lustre or radial (Fig. 4a) and spherical aggregates up to 1 cm consisting of tabular crystals (Fig. 4b) are rare. Azurite as one of the main supergene minerals had usually overgrown older brochantite, strashimirite, olivenite and cornubite, and is covered by younger phases such as euchroite and clinoclase.

Azurite was identified by X-ray powder diffraction and its refined unit-cell parameters correspond well to the published data.

4.1.2. Malachite

Malachite is a common supergene phase occurring as pale to dark-green coatings and crusts or botryoidal aggregates (Fig. 5) with fibrous internal structure and silky lustre. The most common mineral species associated with malachite is azurite. Both are frequently covered by younger aggregates and crystal clusters of euchroite and clinoclase.

It has been confirmed by X-ray powder diffraction. The refined unit-cell parameters correspond to the published data.

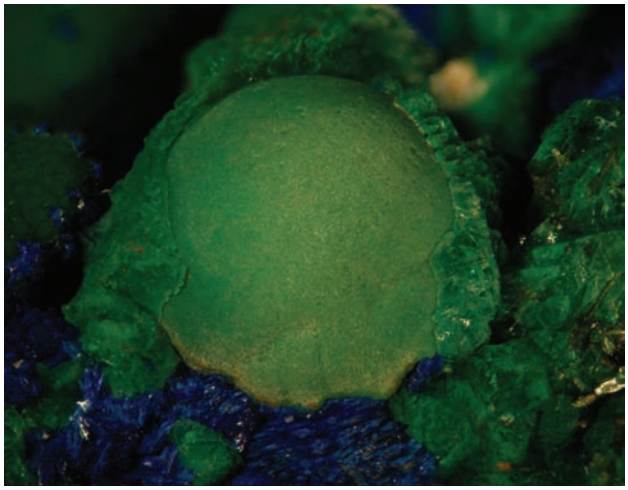

Fig. 5 Hemispherical malachite aggregate partially covered by euchroite. Width of area is 6 mm. Photo by M. Števko.

4.2. Sulphates

4.2.1. Barite

Barite occurs relatively frequently as clusters of thin tabular colourless crystals up to 3 mm covered by bot-

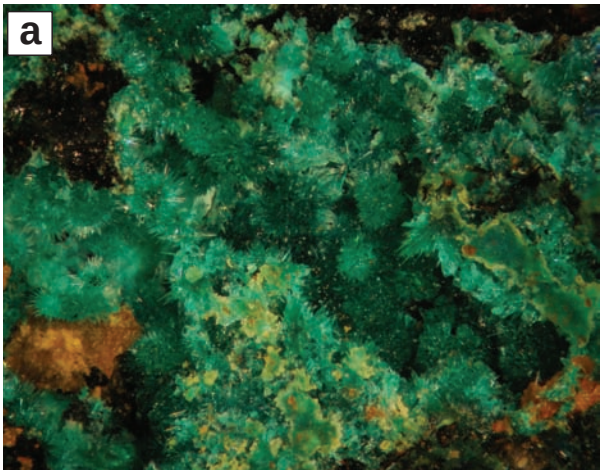

Fig. 6a – Aggregates of prismatic to tabular brochantite crystals. Width of area is 7 mm. Photo by M. Števko. **b –** Radial group of tabular brochantite crystals; SEM photo by M. Števko**.**

Tab. 1 Unit-cell parameters of brochantite (for monoclinic space group P21/a)

Occurrence	Reference	a [Å]	b [Å]	c [Å]	β°	V [Å3]
Farbište, Slovakia	this paper	13.1195(11)	9.8461(12)	6.0157(7)	103.35(1)	756.08(9)
Jáchymov, Czech Republic	Ondruš et al. (1997)	13.445(4)	9.856(6)	6.024(3)	103.42(1)	776.5
Socorro, USA	Helliwell and Smith (1997)	13.087(1)	9.835(1)	6.015(2)	103.3	753.3
Gelnica, Slovakia	Sejkora et al. (2001)	13.128(2)	9.861(1)	6.024(1)	103.27(1)	759.1(2)
Val Fucinaia, Tuscany, Italy	Merlino (2003)	13.140(2)	9.863(2)	6.024(1)	103.16(3)	760.12
Horní Slavkov, Czech Republic	Sejkora et al. (2006)	13.110(9)	9.853(5)	6.015(3)	103.37(4)	755.9

ryoidal chrysocolla or crystalline azurite and malachite crusts. Rarely it is overgrown by bariopharmacosiderite-*Q*, tyrolite and euchroite.

Barite was identified by X-ray powder diffraction and semi-quantitative microprobe analyses confirmed the main components, Ba, S and O.

4.2.2. Brochantite

Brochantite has been identified as rare emerald-green crusts (Fig. 6a) which cover several cm^2 in association with azurite and malachite. Crusts are composed of tiny tabular to prismatic crystals up to 0.2 mm (Fig. 6b), grouped into radial aggregates. Brochantite aggregates are sometimes replaced by parnauite and both are covered by tiny crystals of younger azurite and malachite.

It was identified by X-ray powder diffraction. Its refined unit-cell parameters (Tab. 1) are in good agreement with the data published for this mineral. The chemical composition of brochantite (Tab. 2) is very simple; only the presence of Cu and S is indicated. Empirical formula of brochantite based on S = 1 is $Cu_{3.93}(SO_4)_{1.00}(OH)_{5.85}$.

Tab. 2 Chemical composition of brochantite (in wt. %)

	mean 1–3	1	2	3
CuO	71.85	71.39	71.61	72.55
SO_3	18.41	18.30	18.34	18.60
H_2O*	12.13	12.05	12.09	12.25
total	102.39	101.74	102.04	103.40
Cu^{2+}	3.927	3.926	3.930	3.926
S^{6+}	1.000	1.000	1.000	1.000
OH^-	5.855	5.853	5.859	5.854

1–3: mean and representative analyses of brochantite from Farbište. Coefficients of empirical formula were obtained assuming S = 1; H_2O* contents were calculated on the basis of charge balance.

4.3. Arsenates

4.3.1. Bariopharmacosiderite-Q

This mineral occurs as two morphologically different types. The first is represented by thin yellow to yellowish brown crystalline crusts and coatings in fissures. The second occurs as brittle fillings of vugs (Fig. 7a). Both types of bariopharmacosiderite-*Q* aggregates are composed of well-developed isolated pseudocubic crystals (Fig. 7b) up to 0.7 mm across. Bariopharmacosiderite-*Q* is one of the oldest supergene arsenates and is often covered by strashimirite, olivenite and cornubite.

Bariopharmacosiderite-*Q* has been confirmed by X-ray powder diffraction (Tab. 3) and its refined unit-cell parameters (Tab. 4) fit well with the data published by Hager et al. (2010) for the tetragonal polytype of bariopharmacosiderite. Both types of pharmacosiderite have

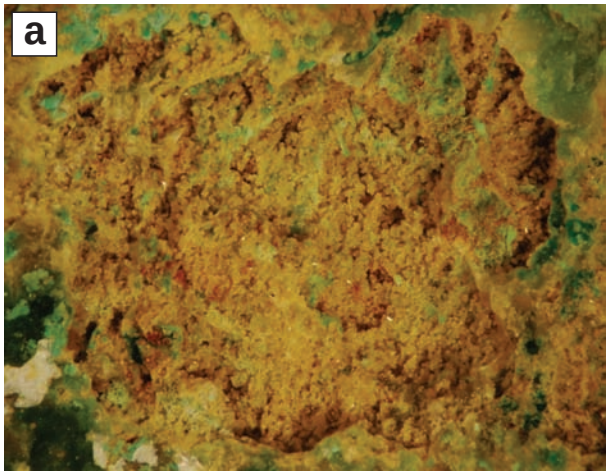
a

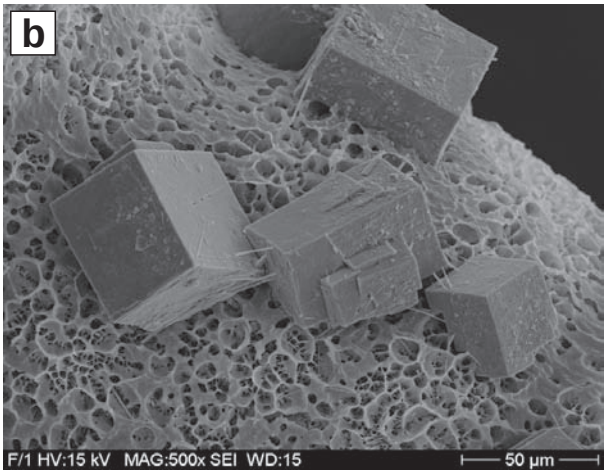
b
F/1 HV:15 kV MAG:500x SEI WD:15
50 µm

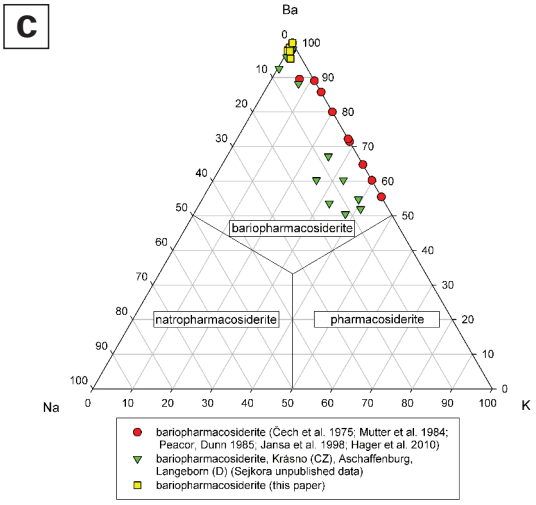
c
Ba
Na
K
bariopharmacosiderite
natropharmacosiderite
pharmacosiderite
bariopharmacosiderite (Čech et al. 1975; Mutter et al. 1984; Peacor, Dunn 1985; Jansa et al. 1998; Hager et al. 2010)
bariopharmacosiderite, Krásno (CZ), Aschaffenburg, Langeborn (D) (Sejkora unpublished data)
bariopharmacosiderite (this paper)

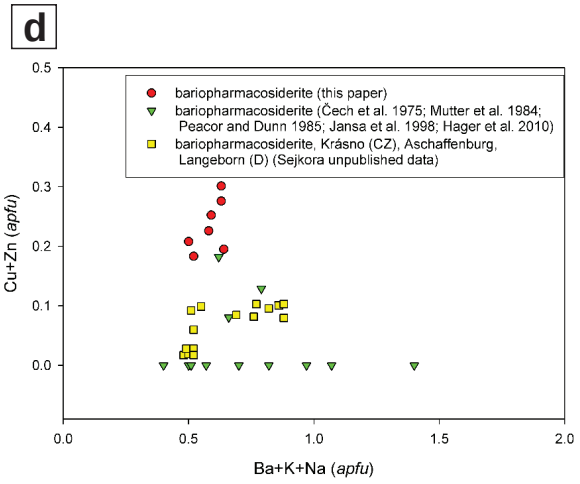
d
bariopharmacosiderite (this paper)
bariopharmacosiderite (Čech et al. 1975; Mutter et al. 1984; Peacor and Dunn 1985; Jansa et al. 1998; Hager et al. 2010)
bariopharmacosiderite, Krásno (CZ), Aschaffenburg, Langeborn (D) (Sejkora unpublished data)
Cu+Zn (apfu)
Ba+K+Na (apfu)

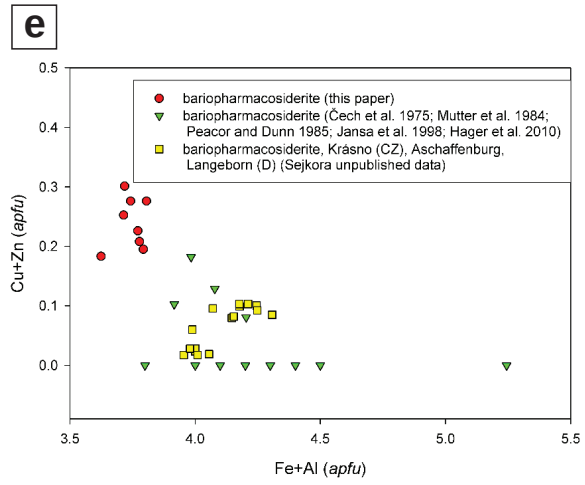
e
bariopharmacosiderite (this paper)
bariopharmacosiderite (Čech et al. 1975; Mutter et al. 1984; Peacor and Dunn 1985; Jansa et al. 1998; Hager et al. 2010)
bariopharmacosiderite, Krásno (CZ), Aschaffenburg, Langeborn (D) (Sejkora unpublished data)
Cu+Zn (apfu)
Fe+Al (apfu)

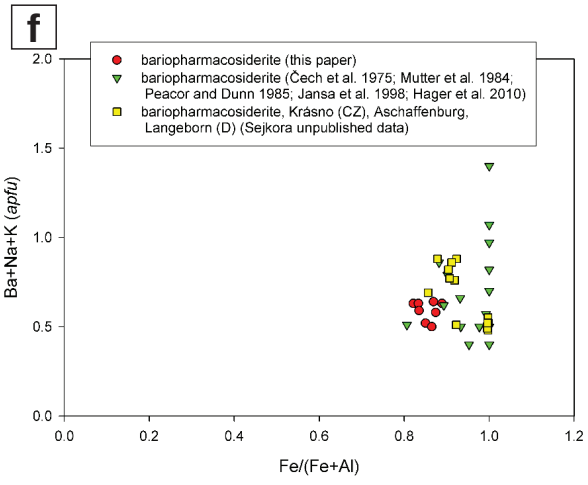
f
bariopharmacosiderite (this paper)
bariopharmacosiderite (Čech et al. 1975; Mutter et al. 1984; Peacor and Dunn 1985; Jansa et al. 1998; Hager et al. 2010)
bariopharmacosiderite, Krásno (CZ), Aschaffenburg, Langeborn (D) (Sejkora unpublished data)
Ba+Na+K (apfu)
Fe/(Fe+Al)

Tab. 3 X-ray powder diffraction pattern of bariopharmacosiderite-*Q*

h	*k*	*l*	$d_{obs.}$	I/I_o	$d_{calc.}$	*h*	*k*	*l*	$d_{obs.}$	I/I_o	$d_{calc.}$
0	0	1	8.11	100	8.06	1	1	3	2.4339	16	2.4222
0	1	0	7.96	70	7.93	3	1	1	2.4017	21	2.3949
0	1	1	5.68	18	5.65	2	2	2	2.3088	21	2.3015
1	1	0	5.63	22	5.61	0	2	3	2.2338	13	2.2237
1	1	1	4.617	35	4.603	2	1	3	2.1499	14	2.1412
0	0	2	4.048	25	4.028	3	1	2	2.1278	16	2.1292
0	2	0	3.977	34	3.966	0	1	4	1.9634	14	1.9522
0	2	1	3.568	20	3.558	2	2	3	1.9470	12	1.9396
1	1	2	3.285	21	3.272	3	2	2	1.9292	12	1.9307
2	1	1	3.256	67	3.246	4	1	1	1.8727	18	1.8711
0	2	2	2.837	42	2.826	4	2	0	1.7773	15	1.7736
2	2	0	2.810	26	2.804	4	1	2	1.7371	13	1.7360
0	0	3	2.719	34	2.686	3	2	3	1.7055	12	1.7018
2	2	1	2.654	24	2.648	4	2	2	1.6289	14	1.6232
0	1	3	2.556	23	2.54375	0	3	4	1.6004	13	1.6022
0	3	1	2.518	23	2.51211	0	5	0	1.5889	12	1.5864

Tab. 4 Unit-cell parameters of bariopharmacosiderite-*Q* (for tetragonal space group *P*–42*m*)

Occurrence	**Reference**	***a* [Å]**	***c* [Å]**	***V* [Å³]**
Farbište, Slovakia	this paper	7.9317(5)	8.0568(7)	506.87(4)
Sunny Corner mine, NSW, Australia	Hager et al. (2010), bariopharmacosiderite-*Q*	7.947(1)	8.049(2)	508.3(1)
Robinson's Reef, Victoria, Australia	Hager et al. (2010), bariopharmacosiderite-*C*#	7.942(1)	–	500.9(1)

– cubic, space group *P*–43*m*

very similar chemical composition (Tab. 5); only minimal contents of K (up to 0.01 *apfu*) and Na (up to 0.02 *apfu*) were detected (Fig. 7c). Interesting are elevated contents of Cu and Zn, which were reported only for bariopharmacosiderite from Cínovec (Jansa et al. 1998). Diagrams in Figs 7d–e suggest that Cu and Zn probably substitute for Fe^{3+} + Al, rather than replacing cations in the Ba + Na + K position. A similar situation for Cu + Zn in the Fe^{3+} + Al position of Pb-dominant minerals of the alunite supergroup was described by, e.g., Sato et al. (2008) and Sejkora et al. (2009). Iron in bariopharmacosiderite from Farbište is partly substituted by Al (0.42–0.68 *apfu*, Fig. 7f). Similar aluminium contents were determined in some bariopharmacosiderite samples from Krásno (Sejkora, unpublished data) or from Záblatíčko (Čech et al. 1975) and Cínovec (Jansa et al. 1998). Dominating As in the anion group of bariopharmacosiderite from Farbište is accompanied by negligible contents of P (up to 0.01 *apfu*) and Si (up to 0.02 *apfu*). Empirical formulae for the two studied types of bariopharmacosiderite from Farbište were calculated on the basis of (As + P + Si) = 3 *apfu* as follows: $(Ba_{0.58}Na_{0.01})_{\Sigma 0.59}(Fe_{3.10}Al_{0.61}Cu_{0.17}Zn_{0.09})_{\Sigma 3.97}(AsO_4)_{2.98}(SiO_4)_{0.02}(OH)_{3.81}\cdot 6H_2O$ and $(Ba_{0.57}Na_{0.01})_{\Sigma 0.58}(Fe_{3.30}Al_{0.48}Cu_{0.13}Zn_{0.09})_{\Sigma 4.00}(AsO_4)_{2.99}(SiO_4)_{0.01}(OH)_{3.91}\cdot 6H_2O$.

⇦

Fig. 7a – Crystalline crusts and fillings of bariopharmacosiderite-Q. Width of area is 5 mm. Photo by M. Števko. **b –** A group of pseudocubic crystals of bariopharmacosiderite-Q on chrysocolla; SEM photo by M. Števko. **c –** Na–Ba–K (atomic ratios) ternary diagram for the Ba-dominant members of the pharmacosiderite group. **d –** A binary plot of Ba + K + Na vs. Cu + Zn (apfu) for Ba-dominant pharmacosiderite minerals. **e –** A binary plot of Fe + Al vs. Cu + Zn (apfu) for Ba-dominant pharmacosiderite minerals. **f –** A binary plot of Fe/(Fe + Al) vs. Ba + Na + K (apfu) for Ba-dominant pharmacosiderite minerals.

4.3.2. Clinoclase

Clinoclase has been found frequently as clusters and coatings of tabular crystals (Fig. 8), usually up to 1 mm in

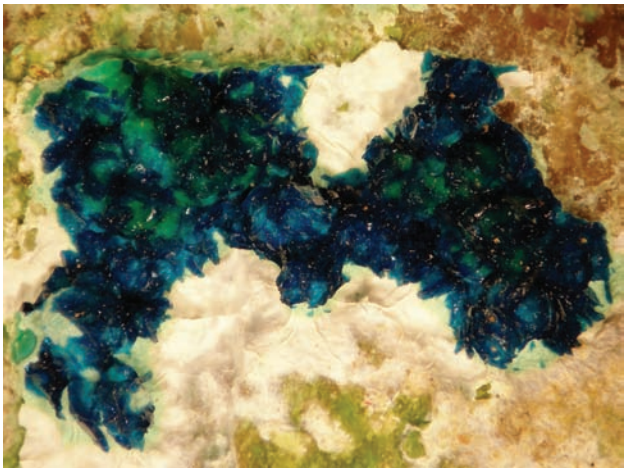

Fig. 8 Aggregates of dark blue clinoclase crystals on strashimirite and white olivenite. Width of area is 7 mm. Photo by M. Števko.

Tab. 5 Chemical composition of bariopharmacosiderite-*Q* (in wt. %)

	mean	1	2	3	mean	4	5	6
Na_2O	0.03	0.00	0.05	0.04	0.04	0.06	0.05	0.00
K_2O	0.00	0.00	0.00	0.00	0.02	0.06	0.00	0.00
BaO	10.61	11.16	11.04	9.63	9.79	10.26	10.24	8.86
CuO	1.56	1.92	2.05	0.70	1.17	0.96	1.58	0.97
ZnO	0.84	0.64	0.77	1.11	0.86	0.76	0.84	0.98
Al_2O_3	3.70	4.02	3.70	3.39	2.71	2.79	2.32	3.03
Fe_2O_3	29.34	28.95	28.93	30.15	29.44	28.89	29.05	30.37
SiO_2	0.10	0.10	0.03	0.18	0.04	0.04	0.00	0.07
As_2O_5	40.63	39.80	40.26	41.82	38.50	37.79	37.71	40.01
P_2O_5	0.02	0.00	0.00	0.05	0.00	0.00	0.00	0.00
H_2O*	16.88	16.94	16.86	16.84	16.04	15.85	15.78	16.50
Total	103.71	103.53	103.69	103.91	98.61	97.46	97.57	100.79
Na^+	0.008	0.000	0.014	0.011	0.011	0.018	0.015	0.000
K^+	0.000	0.000	0.000	0.000	0.004	0.012	0.000	0.000
Ba^{2+}	0.584	0.627	0.616	0.513	0.570	0.609	0.611	0.496
Σ Ba-site	0.592	0.627	0.629	0.523	0.585	0.638	0.625	0.496
Al^{3+}	0.613	0.680	0.621	0.543	0.476	0.498	0.416	0.510
Fe^{3+}	3.101	3.126	3.098	3.082	3.295	3.295	3.326	3.267
Cu^{2+}	0.165	0.208	0.220	0.072	0.131	0.110	0.182	0.105
Zn^{2+}	0.087	0.068	0.081	0.111	0.094	0.085	0.094	0.103
Σ Fe-site	3.967	4.081	4.020	3.807	3.997	3.988	4.018	3.985
Si^{4+}	0.015	0.014	0.004	0.024	0.005	0.006	0.000	0.010
As^{5+}	2.984	2.986	2.996	2.970	2.995	2.994	3.000	2.990
P^{5+}	0.002	0.000	0.000	0.006	0.000	0.000	0.000	0.000
Σ T-site	3.000	3.000	3.000	3.000	3.000	3.000	3.000	3.000
OH	3.810	4.209	4.000	3.250	3.915	4.011	4.015	3.731
H_2O	6.003	6.002	6.003	6.003	6.000	6.005	6.001	6.000

1–3 – representative analyses of crystalline crusts of bariopharmacosiderite; 4–6 – representative analyses of brittle fillings of bariopharmacosiderite from Farbište. Coefficients of empirical formula were obtained assuming (As + P + Si) = 3; H_2O* was calculated from the ideal content in the formula H_2O = 6 and a charge balance.

Tab. 6 Unit-cell parameters of clinoclase (for monoclinic space group $P2_1/b$)

occurrence	reference	*a* [Å]	*b* [Å]	*c* [Å]	*β*°	*V* [Å³]
Farbište, Slovakia	this paper	7.2566(4)	6.4499(4)	12.3741(9)	99.485(7)	571.24(1)
Farbište, Slovakia	Řídkošil (1981b)	7.256(3)	6.459(3)	12.390(5)	99.43(3)	572.8(4)
Novoveská Huta, Slovakia	Řídkošil (1981b)	7.245(3)	6.453(3)	12.385(5)	99.55(4)	570.9(4)
Ľubietová, Slovakia	Řídkošil (1981b)	7.250(4)	6.458(4)	12.393(7)	99.33(5)	572.5(5)
Roughton Gill, England	Eby and Hawthorne (1990)	7.257(2)	6.457(2)	12.378(3)	99.5(0)	572.0
Gelnica, Slovakia	Sejkora et al. (2001)	7.273(3)	6.462(4)	12.401(5)	99.49(4)	574.9(4)

size, and covering areas up to several cm² on fissures and in vugs of mineralized rocks. The crystals are dark-blue to greenish-blue, translucent to transparent with vitreous to pearly lustre. Rare are nearly black, barrel-shaped complex clinoclase aggregates up to 2 mm. Clinoclase is mostly associated with older strashimirite, olivenite and cornubite.

Clinoclase was identified by X-ray powder diffraction. The refined unit-cell parameters (Tab. 6) correspond to the published data. The chemical composition of clinoclase is close to the theoretical end member (Tab. 7). Only some crystals contain slightly increased Zn (up to 0.04 *apfu*), Ni and Co (to 0.01 *apfu*). In the anion site, As is accompanied by minor P (up to 0.02 *apfu*). Interesting are minor contents of F (0.01–0.03 *apfu*), which were not previously reported for this species. The empirical formula for clinoclase from Farbište may be expressed on the basis of (As + P) = 1 *apfu* as $(Cu_{2.97}Zn_{0.01})_{\Sigma 2.98}(AsO_4)_{0.99}(PO_4)_{0.01}(OH)_{2.95}F_{0.02}$.

4.3.3. Cornubite

Cornubite has been identified as abundant, pale to dark-green semi-spherical aggregates (Fig. 9a) up to 3 mm across, with vitreous lustre. The aggregates are usually grouped into

Tab. 7 Chemical composition of clinoclase (in wt. %)

	mean	1	2	3	4	5	6	7	8	9
CuO	60.89	58.96	59.27	61.21	61.23	61.53	61.26	61.10	61.86	61.55
CoO	0.02	0.11	0.11	0.00	0.00	0.00	0.00	0.00	0.00	0.00
NiO	0.01	0.06	0.06	0.00	0.00	0.00	0.00	0.00	0.00	0.00
ZnO	0.28	0.77	0.62	0.06	0.21	0.21	0.22	0.02	0.23	0.19
As_2O_5	29.45	28.53	26.32	29.86	30.09	29.54	29.90	30.15	30.25	30.38
P_2O_5	0.10	0.29	0.29	0.03	0.06	0.06	0.05	0.03	0.05	0.07
F	0.09	0.09	0.05	0.04	0.11	0.09	0.07	0.11	0.08	0.13
H_2O*	6.86	6.70	7.28	6.83	6.76	6.97	6.84	6.69	6.89	6.75
O=F	–0.04	–0.04	–0.02	–0.02	–0.05	–0.04	–0.03	–0.05	–0.03	–0.05
total	97.66	95.47	93.98	98.01	98.41	98.36	98.31	98.05	99.33	99.02
Cu^{2+}	2.970	2.937	3.196	2.957	2.930	2.999	2.952	2.923	2.946	2.916
Co^{2+}	0.001	0.006	0.006	0.000	0.000	0.000	0.000	0.000	0.000	0.000
Ni^{2+}	0.001	0.003	0.003	0.000	0.000	0.000	0.000	0.000	0.000	0.000
Zn^{2+}	0.013	0.038	0.033	0.003	0.010	0.010	0.010	0.001	0.011	0.009
subtotal	2.986	2.984	3.239	2.960	2.940	3.009	2.962	2.924	2.957	2.925
As^{5+}	0.994	0.984	0.982	0.998	0.997	0.997	0.997	0.998	0.997	0.996
P^{5+}	0.006	0.016	0.018	0.002	0.003	0.003	0.003	0.002	0.003	0.004
subtotal	1.000	1.000	1.000	1.000	1.000	1.000	1.000	1.000	1.000	1.000
F^-	0.017	0.019	0.011	0.008	0.022	0.018	0.014	0.022	0.016	0.026
OH^-	2.954	2.949	3.466	2.911	2.858	3.000	2.911	2.826	2.898	2.824
Σ F + OH	2.971	2.968	3.477	2.919	2.880	3.019	2.925	2.848	2.914	2.850

1–9: mean and representative analyses of clinoclase from Farbište. Coefficients of empirical formula were calculated on the basis (As + P) = 1; H_2O* contents based on charge balance.

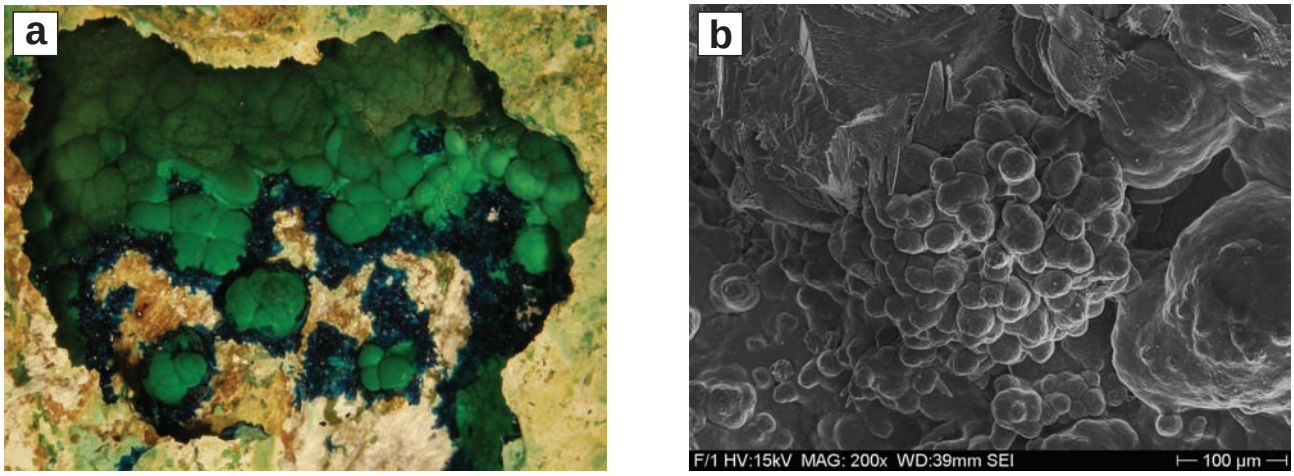

Fig. 9a – Green botryoidal aggregates of cornubite with clinoclase and white olivenite. Width of area is 15 mm. Photo by M. Števko. **b** – Radial aggregate of olivenite crystals completely covered by cornubite crust with characteristic irregular surface. Minor tabular crystals of younger clinoclase are also present; SEM photo by M. Števko.

crusts and coatings without visible crystals on the surface, which usually cover botryoidal aggregates of older strashimirite and clusters of olivenite crystals (Fig. 9b).

Cornubite was identified by X-ray powder diffraction and its refined unit-cell parameters (Tab. 8) are in good agreement with the data published for this mineral. The study of chemical composition of cornubite (Tab. 9) resulted in determination of minor contents of Zn in the range of 0.01–0.05 *apfu* and irregular contents of Ca up to 0.01 *apfu*. Predominating As in the anion group is accompanied by Si (up to 0.06 *apfu*), Sb (up to 0.03 *apfu*) and P (*c.* 0.03 *apfu*). The empirical formula of cornubite calculated on the basis of (As + Si + P + Sb) = 2 is $(Cu_{5.03}Zn_{0.03})_{\Sigma 5.06}(AsO_4)_{1.96}(SiO_4)_{0.03}(SbO_4)_{0.01}(OH)_{4.07}F_{0.04}$.

Tab. 8 Unit-cell parameters of cornubite (for triclinic space space group *P*1)

Occurrence	Reference	*a* [Å]	*b* [Å]	*c* [Å]	*α*°	*β*°	*γ*°	*V* [Å³]
Farbište, Slovakia	this paper	6.1374(8)	6.2559(9)	6.7841(10)	93.071(9)	111.346(8)	107.398(9)	227.60(1)
Reichenbach, Germany	Tillmanns et al. (1985)	6.121(1)	6.251(1)	6.790(1)	92.93(1)	111.30(1)	107.47(1)	227.9
Gelnica, Slovakia	Sejkora et al. (2001)	6.14(1)	6.24(1)	6.80(1)	93.3(1)	111.36(9)	106.8(1)	228(1)

Tab. 9 Chemical composition of cornubite and cornwallite (in wt. %)

	mean 1–8	1	2	3	4	5	6	7	8	mean 9–13	9	10	11	12	13
CaO	0.04	0.00	0.00	0.00	0.00	0.10	0.08	0.00	0.11	0.09	0.06	0.11	0.10	0.10	0.07
CuO	57.75	58.44	58.30	57.26	56.57	57.93	57.81	57.65	58.07	58.26	58.76	58.03	58.05	58.36	58.09
ZnO	0.33	0.20	0.17	0.55	0.55	0.21	0.62	0.16	0.20	0.56	0.36	0.69	0.65	0.62	0.48
Sb_2O_3	0.23	0.34	0.00	0.20	0.18	0.05	0.21	0.72	0.14	0.00	0.00	0.00	0.00	0.00	0.00
SiO_2	0.23	0.23	0.00	0.33	0.52	0.16	0.21	0.19	0.18	0.14	0.23	0.11	0.17	0.08	0.09
As_2O_5	32.48	31.58	32.98	32.21	32.20	33.07	32.84	31.95	32.98	33.16	32.69	32.86	33.40	33.85	33.02
P_2O_5	0.04	0.28	0.00	0.00	0.00	0.00	0.00	0.00	0.00	0.11	0.04	0.14	0.14	0.15	0.10
F	0.11	0.08	0.12	0.08	0.07	0.12	0.16	0.15	0.07	0.10	0.11	0.06	0.09	0.09	0.15
H_2O*	5.30	5.53	5.43	5.26	4.99	5.26	5.31	5.30	5.32	5.37	5.52	5.46	5.27	5.28	5.36
O=F	–0.04	–0.03	–0.05	–0.03	–0.03	–0.05	–0.07	–0.06	–0.03	–0.04	–0.05	–0.03	–0.04	–0.04	–0.06
total	96.45	96.65	96.95	95.86	95.05	96.85	97.17	96.06	97.04	97.75	97.72	97.43	97.83	98.49	97.30
Ca^{2+}	0.004	0.000	0.000	0.000	0.000	0.012	0.010	0.000	0.013	0.011	0.007	0.014	0.012	0.012	0.009
Cu^{2+}	5.034	5.157	5.108	5.014	4.903	5.009	5.000	5.066	5.018	5.009	5.115	5.036	4.940	4.924	5.032
Zn^{2+}	0.028	0.017	0.015	0.047	0.047	0.018	0.052	0.014	0.017	0.047	0.031	0.059	0.054	0.051	0.041
subtotal	5.067	5.175	5.122	5.061	4.950	5.039	5.062	5.080	5.049	5.066	5.153	5.108	5.006	4.987	5.082
Si^{4+}	0.026	0.027	0.000	0.038	0.060	0.018	0.024	0.022	0.021	0.015	0.027	0.013	0.019	0.009	0.010
As^{5+}	1.959	1.929	2.000	1.952	1.932	1.979	1.966	1.943	1.973	1.974	1.970	1.974	1.967	1.977	1.980
P^{5+}	0.003	0.028	0.000	0.000	0.000	0.000	0.000	0.000	0.000	0.011	0.004	0.014	0.013	0.014	0.010
Sb^{5+}	0.011	0.016	0.000	0.010	0.009	0.002	0.010	0.035	0.007	0.000	0.000	0.000	0.000	0.000	0.000
subtotal	2.000	2.000	2.000	2.000	2.000	2.000	2.000	2.000	2.000	2.000	2.000	2.000	2.000	2.000	2.000
F^-	0.039	0.030	0.044	0.029	0.025	0.043	0.058	0.055	0.025	0.036	0.040	0.022	0.032	0.032	0.054
OH^-	4.080	4.310	4.201	4.067	3.819	4.017	4.056	4.113	4.060	4.077	4.243	4.184	3.961	3.934	4.100
∑F + OH	4.118	4.339	4.245	4.097	3.845	4.060	4.114	4.168	4.085	4.113	4.283	4.206	3.993	3.966	4.155

1–8 – mean and representative analyses of cornubite; 9–13 – mean and representative analyses of cornwallite from Farbište. Coefficients of empirical formula were obtained assuming (As + P + Si + Sb) = 1; H_2O* contents based on charge balance.

Tab. 10 Unit-cell parameters of cornwallite (for monoclinic space group $P2_1/c$)

Occurrence	Reference	*a* [Å]	*b* [Å]	*c* [Å]	*β*°	*V* [Å³]
Farbište, Slovakia	this paper	4.6051(2)	5.7591(5)	17.3854(3)	91.93(2)	460.9 (1)
Clara Mine, Germany	Arlt and Armbruster (1999)	4.600(2)	5.757(3)	17.380(6)	91.87(3)	460.04
Gelnica, Slovakia	Sejkora et al. (2001)	4.608(1)	5.765(1)	17.400(4)	92.01(1)	461.9(1)
Horní Slavkov, Czech Republic	Sejkora et al. (2006)	4.5685(4)	5.7708(4)	17.287(1)	93.02(2)	455.1

4.3.4. Cornwallite

Rare cornwallite occurs as emerald to dark-green botryoidal crusts or isolated hemispherical aggregates up to 2 mm with vitreous lustre, which are partially covered by crystalline crusts of azurite and clusters of euchroite crystals. Surfaces of cornwallite aggregates are irregular (Fig. 10), without any visible crystals.

The mineral was identified by X-ray powder diffraction. The refined unit-cell parameters (Tab. 10) correspond to the published data. Chemical composition of cornwallite (Tab. 9) is relatively simple. Zinc was observed in the range of 0.03–0.06 *apfu* ($CuZn_{-1}$ substitution); Si (0.03 *apfu*) and P (to 0.01 *apfu*) accompanying the dominant As in the anion group are the minor substituting elements; some F (0.02–0.05 *apfu*) was also determined. The empirical formula of cornwallite calculated on the basis of (As + Si + P) = 2 is $(Cu_{5.01}Zn_{0.05})_{\Sigma 5.06}(AsO_4)_{1.97}(SiO_4)_{0.02}(PO_4)_{0.01}(OH)_{4.08}F_{0.04}$.

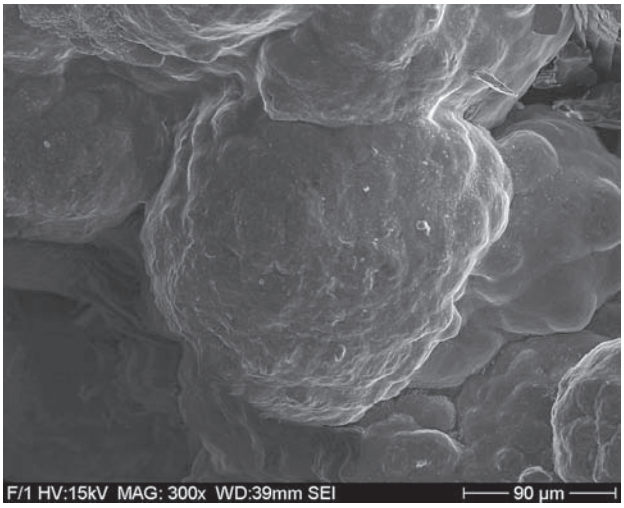

Fig. 10 Irregular surface of cornwallite aggregates; SEM photo by M. Števko.

4.3.5. Euchroite

Euchroite has been found at Farbište as well-developed, short prismatic to thick tabular crystals (Fig. 11a) usually up to 4 mm, exceptionally up to 1 cm in size. The crystals usually occur in clusters which overgrow older azurite, malachite, strashimirite and cornubite crystalline crusts and aggregates on fissures and in vugs of mineralized rocks. Clusters of euchroite crystals sometimes cover areas up to 100 cm^2. Euchroite crystals are of bright emerald-green to leek-green colour, translucent to opaque with a vitreous lustre. Characteristic are euhedral olivenite crystals which are enclosed in euchroite (Fig. 11b). Rare are euchroite crystals completely pseudomorphosed by olivenite or covered by crystalline crusts of younger clinoclase. The second, much rarer form of euchroite, is represented by pale-green hemispherical aggregates up to 2 mm with crystalline surfaces showing minute tabular crystals.

Euchroite has been confirmed by X-ray powder diffraction (Tab. 11). Its refined unit-cell parameters (Tab. 12) are in good agreement with the data given by Eby and Hawthorne (1989) same as Frost et al. (2010). Typical for euchroite in BSE images is parquet-like pattern of fracturing of crystals (Fig. 11b), caused by partial water loss in vacuum. All the three studied types of euchroite have only minimal contents of minor elements (Tab. 13). Characteristic of the first type (leek-to emerald-green crystals with euhedral olivenite inclusions) are P contents in the range 0.06–0.07 *apfu*; its empirical formula on the basis of (As + P) = 1 *apfu* is $Cu_{1.97}(AsO_4)_{0.93}(PO_4)_{0.07}(OH)_{0.91}F_{0.02}\cdot 3H_2O$. The second type of euchroite (pale-green hemispherical aggregates and crystals) contains minor Zn and P (both only up to 0.01 *apfu*). Its empirical formula is $Cu_{1.95}(AsO_4)_{1.00}(OH)_{0.89}F_{0.02}\cdot 3H_2O$. The last type of euchroite (emerald-green crystals and aggregates) is free of minor-elements

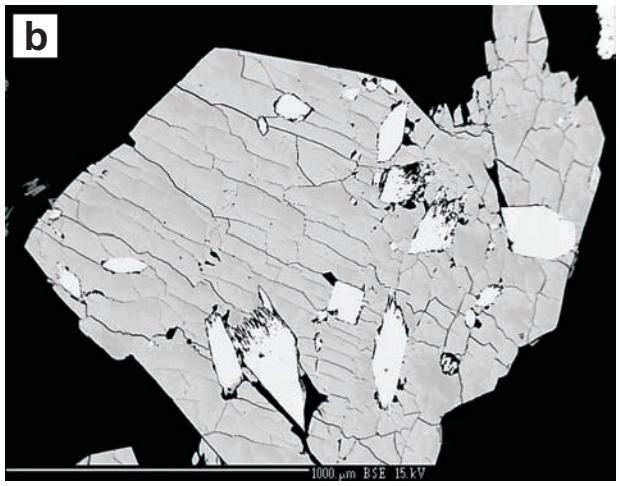

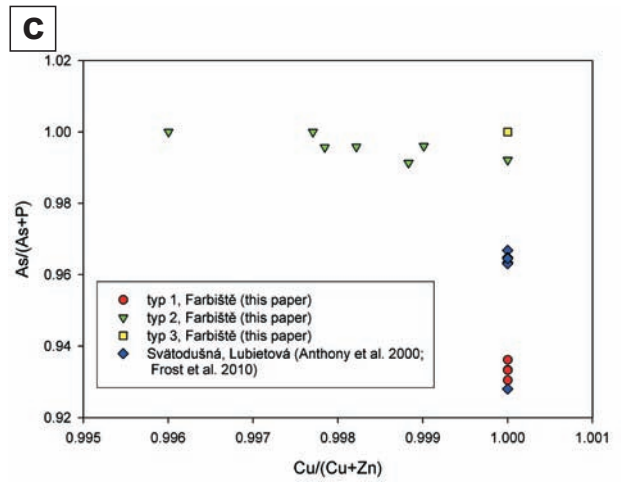

Fig. 11a – A group of short prismatic euchroite crystals on malachite. Width of area is 7 mm. Photo by V. Betz. **b** – Euhedral inclusions of olivenite (white) in euchroite crystal (light grey); BSE photo by J. Sejkora. **c** – A binary plot of Cu/(Cu + Zn) vs. As/(As + P) (*apfu*) for euchroite.

admixture and its empirical formula is $Cu_{1.98}(AsO_4)_{1.00}(OH)_{0.94}F_{0.02}\cdot 3H_2O$. The minor P contents determined in euchroite (Fig. 11c) do not exceed values published for the

Tab. 11 X-ray powder diffraction data of euchroite

h	*k*	*l*	$d_{obs.}$	I/I_o	$d_{calc.}$	*h*	*k*	*l*	$d_{obs.}$	I/I_o	$d_{calc.}$
1	1	0	7.27	100	7.27	1	4	2	1.9535	14	1.9556
0	2	0	5.26	52	5.2872	4	0	2	1.9410	15	1.9430
1	0	1	5.22	90	5.2270	4	3	1	1.9381	16	1.9386
2	0	0	5.03	59	5.0321	5	0	1	1.9115	15	1.9120
2	1	0	4.539	21	4.5391	4	1	2	1.9088	13	1.9107
1	2	1	3.703	66	3.7068	3	3	2	1.8976	14	1.8995
2	1	1	3.642	21	3.6451	0	2	3	1.8968	14	1.9010
2	2	0	3.635	22	3.6353	2	0	3	1.8856	13	1.8897
1	3	0	3.310	17	3.3100	2	1	3	1.8560	15	1.8599
3	1	0	3.196	20	3.1960	2	4	2	1.8517	12	1.8534
2	2	1	3.123	19	3.1250	2	5	1	1.8491	13	1.8495
0	0	2	3.051	19	3.0584	2	2	3	1.7749	12	1.7783
3	0	1	2.940	35	2.9414	5	3	0	1.7455	14	1.7455
0	1	2	2.930	21	2.9367	3	0	3	1.7391	12	1.7424
1	0	2	2.919	17	2.9262	4	4	1	1.7420	14	1.7424
2	3	0	2.876	15	2.8761	3	1	3	1.7158	13	1.7189
3	1	1	2.831	72	2.8326	3	4	2	1.7124	15	1.7138
3	2	0	2.828	46	2.8280	3	5	1	1.7104	16	1.7107
1	1	2	2.813	24	2.8191	1	5	2	1.7064	14	1.7077
0	2	2	2.639	29	2.6436	2	3	3	1.6605	16	1.6633
0	4	0	2.629	46	2.6288	1	6	1	1.6613	17	1.6616
2	0	2	2.609	22	2.6135	5	1	2	1.6590	15	1.6603
2	3	1	2.602	16	2.6027	6	1	0	1.6564	15	1.6564
3	2	1	2.566	23	2.5670	2	6	0	1.6550	13	1.6550
1	2	2	2.552	20	2.5569	3	2	3	1.6511	12	1.6539
1	4	0	2.543	33	2.5434	4	4	2	1.5615	14	1.5625
2	1	2	2.532	16	2.5364	4	5	1	1.5599	13	1.5602
1	4	1	2.3476	19	2.3485	3	3	3	1.5579	12	1.5602
2	2	2	2.3368	16	2.3403	3	5	2	1.5386	12	1.5396
2	4	0	2.3300	22	2.3300	2	4	3	1.5322	11	1.5344
4	0	1	2.3260	16	2.3269	0	6	2	1.5196	13	1.5206
4	1	1	2.2711	22	2.2719	4	2	3	1.5146	15	1.5167
4	2	0	2.2695	23	2.2695	5	3	2	1.5150	14	1.5160
3	3	1	2.2523	17	2.2531	0	1	4	1.5095	14	1.5133
1	3	2	2.2432	12	2.2463	1	0	4	1.5081	13	1.5118
3	1	2	2.2067	16	2.2097	3	6	1	1.5053	14	1.5055
4	2	1	2.1271	13	2.1278	1	6	2	1.5026	13	1.5035
2	3	2	2.0927	12	2.0952	6	1	2	1.4557	14	1.4565
3	2	2	2.0739	12	2.0764	2	6	2	1.4547	13	1.4556
3	4	0	2.0692	14	2.0692	1	2	4	1.4496	13	1.4530
1	5	0	2.0585	18	2.0585	3	4	3	1.4504	12	1.4523
4	3	0	2.0439	15	2.0439	2	1	4	1.4458	12	1.4492
1	1	3	1.9585	16	1.9632	1	5	3	1.4468	11	1.4486
3	4	1	1.9595	17	1.9601						

Tab. 12 Unit-cell parameters of euchroite (for orthorhombic space group $P2_12_12_1$)

Occurrence	**Reference**	***a* [Å]**	***b* [Å]**	***c* [Å]**	***V* [Å^3]**
Farbište, Slovakia	this paper	10.0641(6)	10.5150(6)	6.1167(4)	647.30(7)
Copper Cliff, Montana, USA	Eby and Hawthorne (1989)	10.056(2)	10.506(2)	6.103(2)	644.77
Ľubietová, Slovakia	Frost et al. (2010)	10.053(1)	10.509(1)	6.1086(7)	645.34(9)

Tab. 13 Chemical composition of euchroite (in wt. %)

	mean 1–3	1	2	3	mean 4–9	4	5	6	7	8	9	mean 10–11	10	11
CuO	51.61	49.86	53.31	51.66	50.15	50.10	49.40	49.42	51.17	51.02	49.79	50.78	51.36	50.20
ZnO	0.00	0.00	0.00	0.00	0.09	0.06	0.00	0.05	0.21	0.12	0.11	0.00	0.00	0.00
As_2O_5	35.40	34.42	36.17	35.60	36.94	37.02	36.80	36.41	37.01	37.07	37.34	36.97	37.80	36.13
P_2O_5	1.56	1.45	1.67	1.57	0.10	0.20	0.18	0.09	0.00	0.00	0.10	0.00	0.00	0.00
F	0.14	0.15	0.12	0.15	0.14	0.12	0.15	0.15	0.11	0.15	0.16	0.15	0.17	0.12
H_2O*	20.54	19.87	21.18	20.70	20.04	20.09	19.84	19.73	20.29	20.23	20.05	20.13	20.45	19.81
O=F	–0.06	–0.06	–0.05	–0.06	–0.06	–0.05	–0.06	–0.06	–0.05	–0.06	–0.07	–0.06	–0.07	–0.05
total	109.19	105.69	112.40	109.62	107.40	107.54	106.31	105.79	108.74	108.53	107.48	107.96	109.71	106.21
Cu^{2+}	1.966	1.959	1.981	1.957	1.953	1.938	1.924	1.953	1.997	1.988	1.918	1.985	1.963	2.007
Zn^{2+}	0.000	0.000	0.000	0.000	0.003	0.002	0.000	0.002	0.008	0.005	0.004	0.000	0.000	0.000
As^{5+}	0.933	0.936	0.930	0.933	0.996	0.991	0.992	0.996	1.000	1.000	0.996	1.000	1.000	1.000
P^{5+}	0.067	0.064	0.070	0.067	0.004	0.009	0.008	0.004	0.000	0.000	0.004	0.000	0.000	0.000
F^-	0.022	0.025	0.019	0.024	0.023	0.019	0.024	0.025	0.018	0.024	0.026	0.024	0.027	0.020
OH^-	0.909	0.894	0.944	0.890	0.890	0.862	0.824	0.885	0.993	0.961	0.819	0.946	0.899	0.995
ΣF + OH	0.932	0.918	0.962	0.913	0.913	0.881	0.848	0.910	1.011	0.986	0.844	0.969	0.926	1.015
H_2O	3.000	3.001	3.004	3.017	3.001	3.001	3.000	3.000	3.001	3.000	3.001	3.001	3.002	3.000

means and representative analyses for euchroite from Farbište.
1–3: leek- to emerald-green crystals; 4–9: pale-green hemispherical aggregates and crystals; 10–11: emerald-green crystals and aggregates.
Coefficients of empirical formula were obtained assuming (As + *P*) = 1; H_2O* contents were calculated on the basis of H_2O = 3 and a charge balance.

same mineral from Svätodušná deposit, Lubietová, Slovak Republic (Anthony et al. 2000; Frost et al. 2010). Interesting is the F content of 0.02–0.03 *apfu* in all types of the studied samples, as such elevated fluorine concentrations were not reported as yet for this species.

4.3.6. Olivenite

Olivenite occurs in fissures of mineralized rocks with other arsenates in three morphologically different types. The first, most abundant one are white to pale-green fibrous coatings (Fig. 8) and radial aggregates with silky lustre. The second habit is short to long prismatic or tabular olive to dark-green crystals (Figs 12a–b) up to 3 mm, enclosed in euchroite or forming isolated clusters and crystalline crusts. Such crystals sometimes completely replace euchroite. The third form of olivenite occurs as olive to pale-green acicular crystals (Fig. 12c) up to 2 mm in size, which are usually grouped to spherical aggregates and crusts. Two generations of olivenite were principally observed. Olivenite I (white fibrous, prismatic or acicular) is older than strashimirite and is often overgrown by cornubite, euchroite and clinoclase. Younger olivenite II is represented by prismatic to tabular crystals, which are exclusively enclosed in euchroite and sometimes even completely replace crystals of this mineral.

Each type of olivenite was identified by X-ray powder diffraction. The refined unit-cell parameters (Tab. 14) correspond well with the data published for this species. Chemical compositions of two olivenite generations were determined (Tab. 15). The first (prismatic crystals enclosed in euchroite) contains only minor Zn and P (up to 0.01 *apfu*). Its empirical formula on the basis of (As + P) = 1 is $Cu_{2.02}(AsO_4)_{0.99}(PO_4)_{0.01}(OH)_{1.02}F_{0.02}$. The second (acicular crystals on strashimirite) contains Zn (up to 0.02 *apfu*) and Al (up to 0.01 *apfu*). The dominant As in the anion group is substituted by a small amount of Sb (up to 0.01 *apfu*). Phosphorus content resulting from otherwise common PAs_{-1} substitution was not detected. The empirical formula of olivenite based on (As + Sb) = 1 is $(Cu_{2.00}Zn_{0.01}Al_{0.01})_{\Sigma 2.02}(AsO_4)_{0.99}(SbO_3OH)_{0.01}(OH)_{1.01}F_{0.02}$. Minor contents of F (0.02–0.03 *apfu*) in both types of olivenite are interesting as no report on fluorine presence in olivenite was found in the literature.

Tab. 14 Unit-cell parameters of olivenite (for orthorhombic space group *Pnnm*)

Occurrence	Reference	*a* [Å]	*b* [Å]	*c* [Å]	*V* [Å³]
Farbište, Slovakia	this paper (white fibrous)	8.2151(7)	8.6080(7)	5.9193(5)	418.59(6)
Farbište, Slovakia	this paper (prismatic crystals)	8.2189(7)	8.6111(7)	5.9209(5)	419.05(3)
Cornwall, England	Burns and Hawthorne (1995)	8.2076(2)	8.5894(2)	5.9286(1)	417.9
Gelnica, Slovakia	Sejkora et al. (2001)	8.245(2)	8.633(2)	5.940(1)	422.8(1)
Majuba Hill, Nevada, USA	Li et al. (2008)	8.2084(3)	8.5844(3)	5.9258(2)	417.56(3)

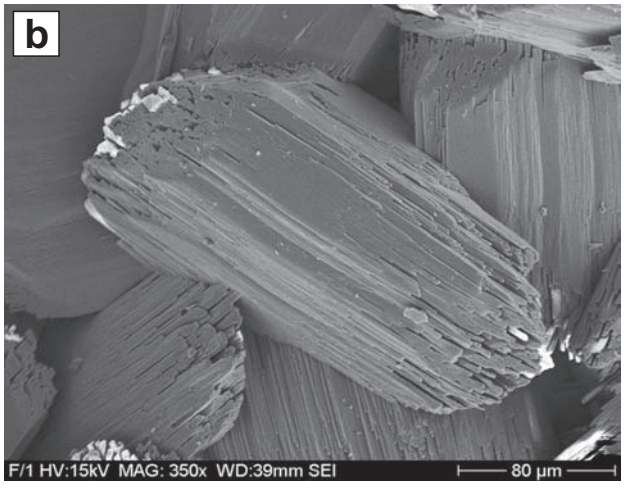

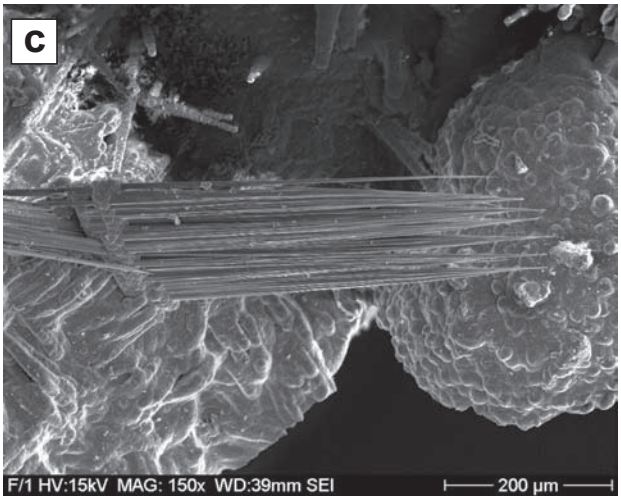

Fig. 12a – Aggregates of tabular olivenite crystals covered by hemispherical aggregates of malachite. Width of area is 10 mm. **b** – A group of prismatic olivenite crystals; SEM. **c** – Aggregate of acicular olivenite crystals partially covered by cornubite; SEM All photos by M. Števko.

4.3.7. Parnauite

Very rare parnauite has been identified as blue-green crystalline coatings which have replaced crystalline aggregates of brochantite (Fig. 13a), or as thin crusts composed of tiny platy crystals in association with strashimirite and euchroite.

Parnauite has been confirmed by X-ray powder diffraction (Tab. 16). Its refined unit-cell parameters (Tab. 17) are in good agreement with the data given by Wise (1978) and Frost et al. (2009a). The crystal structure has not been determined yet but the following ideal formula has been proposed: $Cu_9(AsO_4)_2(SO_4)(OH)_{10}\cdot 7H_2O$ (Wise 1978; Frost et al. 2009a). The possible presence of carbonate groups, reported by Wise (1978) for material from the Majuba Hill mine, was not confirmed by a detailed spectroscopic study of parnauite from the Svätodušná deposit (Frost et al. 2009a). Parnauite from Farbište contains, in contrast to other known analyses of this species, elevated Zn of 0.39–0.46 *apfu* (Fig. 13b) and significantly lower contents of other minor elements. The sum of Ca + Fe + Co + Ni + Al varies between 0.06 and 0.09 *apfu* (Fig. 13c). The composition of the anion group in parnauite from Farbište is near to an ideal one (Fig. 13d), whereas parnauite from the Majuba Hill mine (Wise 1978) and Svätodušná deposit (Frost et al. 2009a) exhibits an As-deficiency and notably increased P contents. The chemical composition of parnauite from Farbište (Tab. 18) based on (As + P + S + Si + Sb) = 3 *apfu* corresponds to an empirical formula $(Cu_{9.08}Zn_{0.41}Fe_{0.02}Al_{0.02}Co_{0.02}Ni_{0.01}Ca_{0.01})_{\Sigma 9.57}\ [(AsO_4)_{2.06}(PO_4)_{0.01}]_{\Sigma 2.07}[(SO_4)_{0.88}(SbO_3OH)_{0.04}(SiO_4)_{0.02}]_{\Sigma 0.94}(OH)_{11.03}\cdot 7H_2O$.

4.3.8. Strashimirite

Strashimirite occurs frequently as pale green to white botryoidal crusts (Fig. 14a) which cover several cm^2 and form isolated hemispherical aggregates up to 3 mm. Typical are a fibrous internal structure and a pearly lustre due to surfaces covered by tiny acicular to platy crystals (Fig. 14b). As one of the oldest arsenate minerals on the locality, strashimirite is usually overgrown by younger olivenite, cornubite, euchroite and clinoclase, and also by azurite and malachite crusts. Strashimirite has been confirmed by X-ray powder diffraction (Tab. 19). Its refined unit-cell parameters (Tab. 20) are in good agreement with the published data. However, Frost et al. (2009b) reported lower values, particularly for parameters *a* and *b*, for samples from Zálesí and Svätodušná deposits. Strashimirite crystal structure remains undetermined and the ideal formula proposed is $Cu_8(AsO_4)_4(OH)_4\cdot 5H_2O$ (Minčeva-Stefanova 1998; Frost et al. 2009b). Two morphological varieties of strashimirite occur at Farbište.

Tab. 15 Chemical composition of olivenite (wt. %)

	mean 1–3	1	2	3	mean 4–8	4	5	6	7	8
CuO	55.90	56.03	56.03	55.64	54.90	54.99	54.44	54.78	55.14	55.13
ZnO	0.09	0.00	0.11	0.17	0.22	0.12	0.14	0.19	0.42	0.23
Al_2O_3	0.00	0.00	0.00	0.00	0.15	0.18	0.25	0.23	0.06	0.05
Sb_2O_3	0.00	0.00	0.00	0.00	0.54	0.37	0.38	0.64	0.64	0.67
As_2O_5	39.66	39.47	39.54	39.96	39.17	39.01	39.60	39.25	38.72	39.29
P_2O_5	0.18	0.19	0.14	0.21	0.00	0.00	0.00	0.00	0.00	0.00
F	0.14	0.17	0.14	0.12	0.15	0.17	0.12	0.18	0.12	0.16
H_2O*	3.22	3.26	3.30	3.11	3.21	3.28	3.08	3.18	3.37	3.17
O=F	–0.06	–0.07	–0.06	–0.05	–0.06	–0.07	–0.05	–0.08	–0.05	–0.07
total	99.13	99.05	99.20	99.16	98.28	98.05	97.96	98.37	98.42	98.63
Cu^{2+}	2.022	2.035	2.036	1.995	2.003	2.021	1.971	1.991	2.031	2.000
Zn^{2+}	0.003	0.000	0.004	0.006	0.008	0.004	0.005	0.007	0.015	0.008
Al^{3+}	0.000	0.000	0.000	0.000	0.009	0.010	0.014	0.013	0.003	0.003
subtotal	2.025	2.035	2.039	2.001	2.019	2.036	1.990	2.011	2.049	2.011
Sb^{3+}	0.000	0.000	0.000	0.000	0.011	0.007	0.008	0.013	0.013	0.013
As^{5+}	0.993	0.992	0.994	0.992	0.989	0.993	0.992	0.987	0.987	0.987
P^{5+}	0.007	0.008	0.006	0.008	0.000	0.000	0.000	0.000	0.000	0.000
subtotal	1.000	1.000	1.000	1.000	1.000	1.000	1.000	1.000	1.000	1.000
F^-	0.022	0.026	0.021	0.018	0.023	0.026	0.018	0.027	0.019	0.024
OH^-	1.028	1.044	1.058	0.983	1.035	1.064	0.984	1.019	1.097	1.014
ΣF + OH	1.050	1.070	1.079	1.001	1.058	1.090	1.002	1.047	1.115	1.039

Mean and representative analyses of 1–3: prismatic crystals of olivenite enclosed in euchroite; 4–8: acicular crystals of olivenite on strashimirite.
Coefficients of empirical formula were obtained assuming (As + P + Sb) = 1; H_2O* contents were calculated on the basis of charge balance.

Tab. 16 X-ray powder diffraction pattern of parnauite from Farbište

h	*k*	*l*	$d_{obs.}$	I/I_o	$d_{calc.}$
0	1	0	14.30	100	14.30
1	1	0	10.40	29	10.36
0	2	0	7.14	8	7.14
1	2	0	6.42	3	6.45
1	0	1	5.61	1	5.59
0	3	0	4.729	2	4.759
1	3	0	4.530	57	4.537
2	3	0	3.990	20	4.021
0	4	0	3.520	4	3.569
3	3	0	3.440	5	3.452
5	1	0	2.929	4	2.944
0	5	0	2.848	16	2.855
1	5	0	2.797	6	2.805
2	5	0	2.657	3	2.669
3	0	2	2.568	5	2.580
3	1	2	2.534	5	2.539
5	3	0	2.522	6	2.543
4	0	2	2.3302	2	2.3495
4	1	2	2.3146	1	2.3183
3	3	2	2.2360	4	2.2682
5	4	1	2.1389	2	2.1487
1	7	0	2.0973	1	2.0209

The first forms fine fibrous aggregates similar to samples from the localities Svätodušná and Zálesí (Frost et al. 2009b). The totals of chemical analyses including calculated contents of H_2O vary in the range 104–108 wt. %. The second variety forms compact aggregates with distinct concentric zoning seen in BSE images (Fig. 14c). Detailed observations and quantitative chemical analyses prove that the zoning corresponds to micro-porosity variations in the studied strashimirite and is not related to variation in chemical composition. Totals of chemical analyses for this type of strashimirite, including theoretical amount of H_2O, vary in the range 110–118 wt. %.

The chemical compositions of both types of strashimirite are closely similar (Tab. 21). The cation positions are occupied by dominating Cu with minor Zn, Ca, Fe, Al and Pb (total of minor elements is 0.09–0.38 *apfu*); similar compositions were reported in other published analyses of this mineral (Fig. 14d). Strashimirite from Farbište differs only by the limited content of Zn (up to 0.20 *apfu*) and lower contents of other elements such as Ni, Co or Ca (Fig. 14e). In anion sites the dominating As is accompanied by minor S (up to 0.12 *apfu*), Sb and Si (up to 0.06 *apfu*), and P (up to 0.05 *apfu*). Similar contents of minor elements were reported in strashimirite from the Zálesí and Svätodušná deposits (Frost et al. 2009b). On the other hand, F determined in strashimirite from Farbište (0.07–0.12 *apfu*) was not noted as yet for this species. The empirical formula for both varieties of strashimirite was calculated on the basis of (As + P + Si + S + Sb) = 4 as follows: $(Cu_{8.05}Zn_{0.12}Al_{0.04}Ca_{0.03})_{\Sigma 8.24}(AsO_4)_{3.87}(SO_4)_{0.06}(SiO_4)_{0.03}(SbO_4)_{0.02}(PO_4)_{0.02}(OH)_{4.43}F_{0.10}\cdot 5H_2O$ (fibrous) and $(Cu_{8.37}Zn_{0.18}Fe_{0.05}Ca_{0.04}Al_{0.03}Pb_{0.01})_{\Sigma 8.68}(AsO_4)_{3.91}(SiO_4)_{0.04}(SO_4)_{0.02}(PO_4)_{0.02}(SbO_4)_{0.01}(OH)_{5.29}F_{0.10}\cdot 5H_2O$ (compact aggregates).

4.3.9. Tyrolite

Tyrolite is typical and the most abundant arsenate at this locality, especially at the dump of the upper adit. It forms radial aggregates (Fig. 15a) up to 1 cm across with a char-

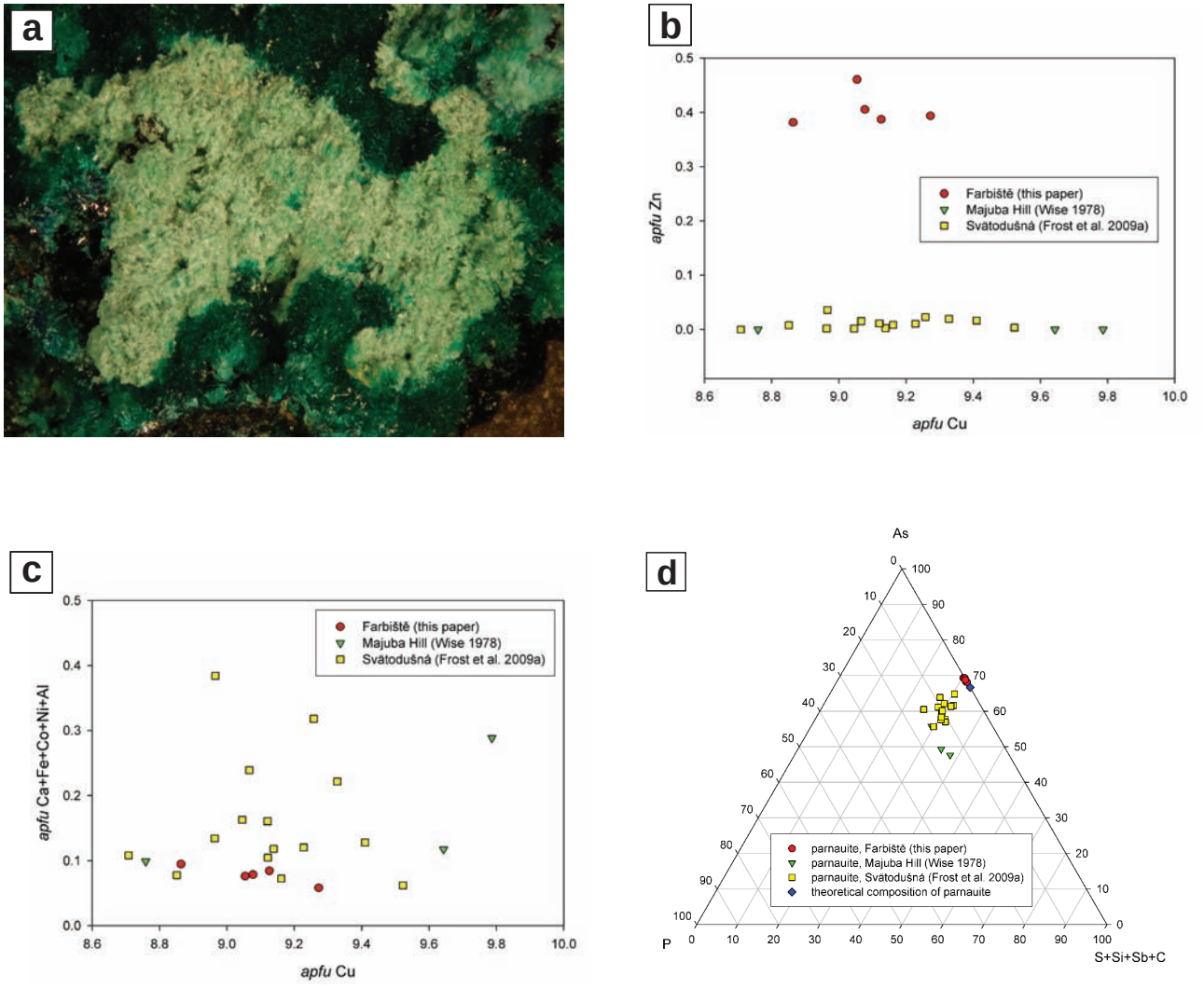

Fig. 13a – Blue-green parnauite crystalline aggregates replacing brochantite. Width of area is 5 mm. Photo by M. Števko. **b** – A binary plot of Cu vs. Zn (*apfu*) for parnauite. **c** – A binary plot of Cu vs. Ca + Fe + Co + Ni + Al (*apfu*) for parnauite. **d –** The P–As–(S + Si + Sb + C) (atomic ratios) ternary plot for parnauite.

Tab. 17 Unit-cell parameters of parnauite (for orthorhombic space group $P2_122$)

Occurrence	Reference	*a* [Å]	*b* [Å]	*c* [Å]	*V* [Å³]
Farbište, Slovakia	this paper	14.887(14)	14.239(7)	6.055(3)	1283.6(11)
Majuba Hill, Nevada, USA	Wise (1978)	14.98(1)	14.223(8)	6.018(8)	1282.2
Ľubietová, Slovakia	Frost et al. (2009a)	14.915(7)	14.190(5)	6.003(4)	1270.5(9)

acteristic pearly lustre, in fissures of mineralized rocks, mostly in association with chrysocolla, azurite and barite. Two different colour-types of tyrolite were observed: emerald to grass green and pale blue-green aggregates. In vugs, the tyrolite occurs rarely also as hemispherical or irregular aggregates of well developed platy to tabular crystals (Fig. 15b) which are sometimes covered with, or replaced by, thin botryoidal coatings of chrysocolla.

Tyrolite was identified using X-ray powder diffraction (Tab. 22) and refined unit-cell parameters of both colour types (Tab. 23). The data obtained fit well with those published by Krivovichev et al. (2006) for the polytype 1*M*. Data given for the 2*M* polytype (Krivovichev et al. 2006) and the discredited $(SO_4)^{2-}$ analogue of tyrolite, clinotyrolite (Ma et al. 1980) are clearly different. The chemical composition of tyrolite has not been completely clarified yet, especially with respect to the role of $(CO_3)^{2-}$ and $(SO_4)^{2-}$ groups. Recent papers, e.g. Krivovichev et al. (2006), proposed an ideal formula of $Ca_2Cu_9(AsO_4)_4(CO_3)(OH)_8 \cdot 11–12H_2O$, with H_2O and carbonate groups significantly disordered in the interlayer of the crystal structure. The chemical analyses of

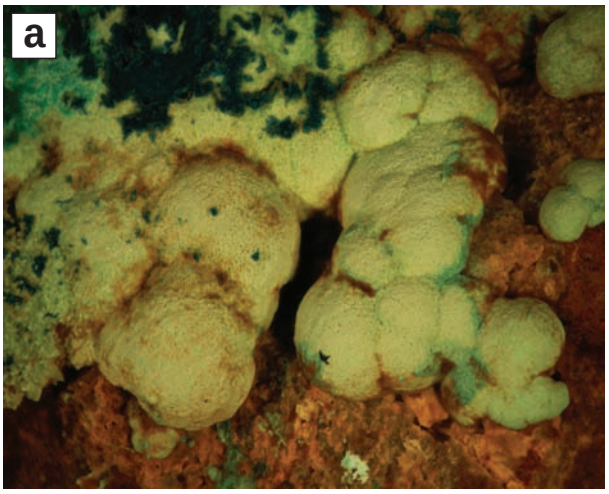

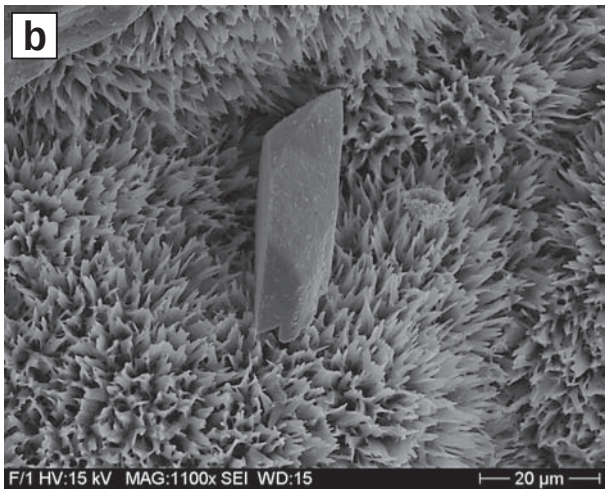

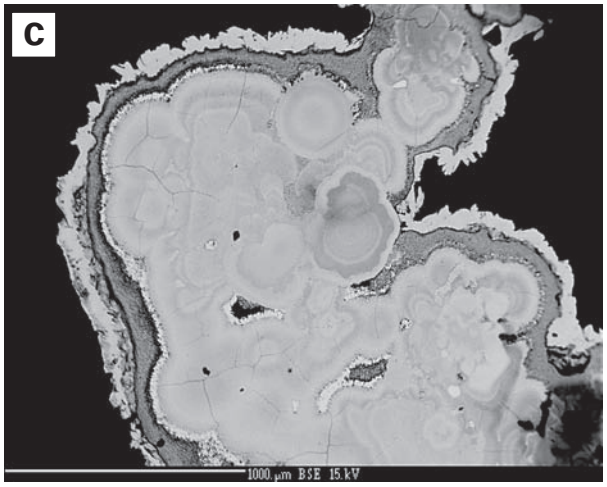

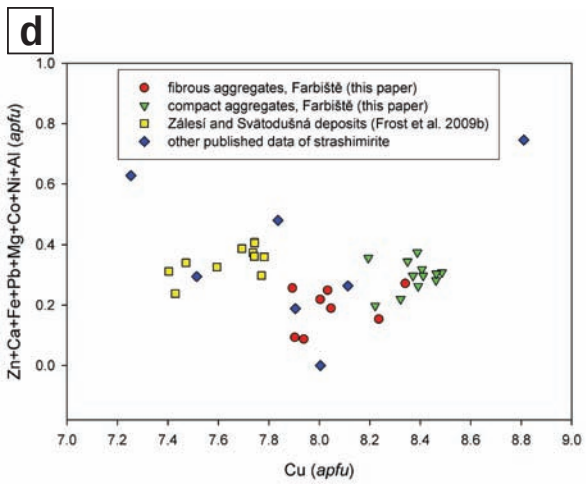

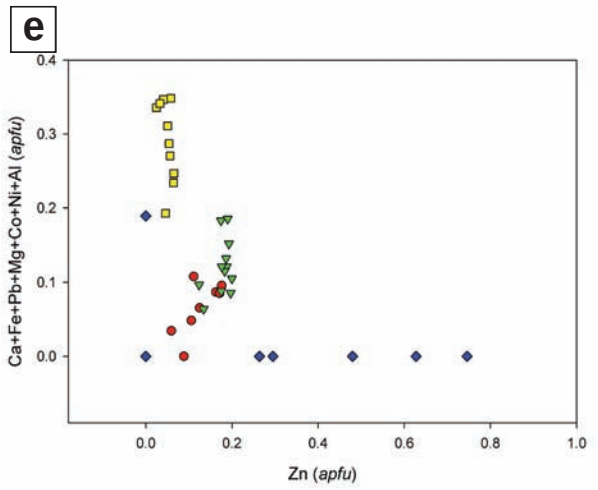

Fig. 14a – Botryoidal strashimirite aggregates partially covered by clinoclase crystalline crusts. Width of area is 8 mm. Photo M. Števko. **b** – Detail of the surface of strashimirite crystal aggregate showing platy crystals with attached tabular crystal of clinoclase; SEM photo by M. Števko. **c** – Compact central part of strashimirite aggregate (light grey) with porous surface layer (grey) covered by clinoclase (white); BSE photo by J. Sejkora. **d** – A binary plot of Cu vs. Zn + Ca + Fe + Pb + Mg + Co + Ni + Al (*apfu*) for strashimirite. Other published data: Novoveská Huta, Slovak Republic (Řídkošil 1978), Zapachitsa, Bulgaria (Minčeva-Stefanova 1968), Venetsa, Bulgaria (Minčeva-Stefanova 1998), Rędziny, Poland (Gołębiowska 1999). **e** – A binary plot of Zn vs. Ca +Fe + Pb + Mg + Co + Ni + Al (*apfu*) for strashimirite. Other published data: Novoveská Huta, Slovak Republic (Řídkošil 1978), Zapachitsa, Bulgaria (Minčeva-Stefanova 1968), Venetsa, Bulgaria (Minčeva-Stefanova 1998), Rędziny, Poland (Gołębiowska 1999).

Tab. 18 Chemical composition of parnauite (in wt. %)

	mean	1	2	3	4
CaO	0.05	0.05	0.06	0.04	0.06
FeO	0.12	0.00	0.09	0.29	0.10
CuO	58.73	59.21	59.23	58.64	57.84
CoO	0.13	0.13	0.13	0.10	0.15
NiO	0.05	0.05	0.05	0.06	0.05
ZnO	2.68	2.57	2.57	2.58	3.01
Al_2O_3	0.07	0.07	0.11	0.05	0.05
Sb_2O_3	0.43	0.40	0.37	0.45	0.48
SiO_2	0.11	0.19	0.06	0.09	0.08
As_2O_5	19.28	18.88	19.50	19.88	18.86
P_2O_5	0.03	0.04	0.07	0.00	0.00
SO_3	5.70	5.61	5.65	5.76	5.78
H_2O*	18.34	18.32	18.45	18.41	18.17
total	105.71	105.52	106.34	106.35	104.63
Ca^{2+}	0.012	0.011	0.013	0.009	0.013
Fe^{2+}	0.021	0.000	0.015	0.049	0.017
Cu^{2+}	9.077	9.272	9.126	8.863	9.054
Co^{2+}	0.021	0.022	0.021	0.016	0.025
Ni^{2+}	0.009	0.008	0.008	0.010	0.008
Zn^{2+}	0.405	0.393	0.387	0.381	0.461
Al^{3+}	0.017	0.017	0.026	0.012	0.012
subtotal	9.561	9.724	9.597	9.339	9.591
Sb^{3+}	0.036	0.034	0.031	0.037	0.041
Si^{4+}	0.021	0.039	0.012	0.018	0.017
As^{5+}	2.063	2.047	2.080	2.080	2.043
P^{5+}	0.005	0.007	0.012	0.000	0.000
S^{6+}	0.875	0.873	0.865	0.865	0.899
subtotal	3.000	3.000	3.000	3.000	3.000
OH^-	11.028	11.333	11.105	10.574	11.117
H_2O	7.002	7.001	6.999	6.999	7.000

1–4 – mean and representative analyses of parnauite from Farbište. Coefficients of empirical formula were obtained assuming (As + P + S + Si + Sb) = 3; H_2O* contents were calculated on the basis of H_2O = 7 and charge balance.

tyrolite from Farbište (Tab. 24) suggest that S does not participate in the As + P group but probably enters the interlayer space together with H_2O and $(CO_3)^{2-}$ groups. The chemical data show a slight difference between the two types of tyrolite. The emerald-green platy crystals

Tab. 19 X-ray powder diffraction data of strashimirite

h	*k*	*l*	$d_{obs.}$	I/I_o	$d_{calc.}$
0	1	0	18.6	100	18.7
0	2	0	9.53	30	9.36
0	0	1	8.97	38	8.96
0	1	1	8.07	14	8.08
1	0	1	6.19	10	6.19
–1	2	1	5.60	9	5.58
2	0	0	4.762	23	4.784
–1	3	1	4.613	11	4.646
–2	0	1	4.440	10	4.442
1	4	0	4.225	15	4.204
0	6	0	3.127	22	3.120
2	5	0	2.985	21	2.948
–1	6	1	2.833	28	2.847
1	5	2	2.688	10	2.696
3	4	0	2.645	13	2.636
2	6	1	2.4688	16	2.4668
–4	0	1	2.3981	11	2.3816
–4	4	0	2.1307	8	2.1300
3	1	3	2.0690	7	2.0508
–1	7	3	1.9762	7	1.9815
3	4	3	1.8670	7	1.8879
2	10	1	1.6976	7	1.6976

with chrysocolla are characterised by increased S in the range 0.20–0.30 *apfu* and relatively low calculated contents of the carbonate groups (0.08–0.17 *apfu*). Its empirical formula on the basis of (As + P) = 4 *apfu* is $Ca_{1.87}(Cu_{8.46}Zn_{0.03})_{\Sigma 8.49}(AsO_4)_{3.91}(PO_4)_{0.09}(SO_4)_{0.25}(CO_3)_{0.11}(OH)_{7.91}F_{0.10}\bullet 11H_2O$. The pale blue-green radial aggregates contain significantly less S (0.04–0.09 *apfu*) and the calculated contents of the carbonate groups are 0.31–0.64 *apfu*. The empirical formula on the basis of (As + P) = 4 *apfu* is $Ca_{1.92}(Cu_{8.57}Zn_{0.03})_{\Sigma 8.60}(AsO_4)_{3.91}(PO_4)_{0.09}(CO_3)_{0.47}(SO_4)_{0.05}(OH)_{7.90}F_{0.10}\cdot 11H_2O$. Both types of tyrolite show minor contents of Zn (0.02–0.04 *apfu*), P (0.08–0.10 *apfu*) and F (0.07–0.13 *apfu*). The differences in composition of the two types of tyrolite are observed in infrared absorption spectra (Figs 15c–d), especially in the 1200–800 cm^{-1} region (Fig. 15d). According to data published by Kloprogge and

Tab. 20 Unit-cell parameters of strashimirite (for monoclinic space group $P2_1/m$)

Occurrence	Reference	*a* [Å]	*b* [Å]	*c* [Å]	*β*°	*V* [Å³]
Farbište, Slovakia	this paper	9.70(2)	18.77(2)	8.99(2)	96.9(1)	1625(3)
Zapachitsa, Bulgaria	Minčeva-Stefanova (1968)	9.70	18.90	9.127	97.12	1660.6
Jáchmov, Czech Republic	Ondruš et al. (1997)	9.71(3)	18.93(7)	8.91(8)	97.1(1)	1625.2
Rędziny, Poland	Gołębiowska (1999)	9.719(2)	18.806(5)	8.937(3)	97.31(3)	1620.2
Zálesí, Czech Republic	Frost et al. (2009b)	9.56(1)	18.38(3)	9.10(1)	97.26(9)	1587(4)
Ľubietová, Slovakia	Frost et al. (2009b)	9.524(3)	18.536(6)	9.058(4)	96.96(4)	1587.1(9)

Tab. 21 Chemical composition of strashimirite (in wt. %)

	mean [a]	1	2	3	4	5	mean [b]	6	7	8	9	10
CaO	0.14	0.16	0.11	0.12	0.34	0.00	0.20	0.20	0.26	0.19	0.21	0.27
FeO	0.00	0.00	0.00	0.00	0.00	0.00	0.30	0.20	0.37	0.16	0.65	0.61
PbO	0.00	0.00	0.00	0.00	0.00	0.00	0.11	0.00	0.26	0.17	0.09	0.00
CuO	54.77	55.57	55.70	54.20	54.17	53.86	58.35	57.60	60.54	57.18	58.92	59.21
ZnO	0.87	1.15	0.73	0.77	1.17	0.61	1.26	1.37	1.43	1.38	1.28	1.37
Al_2O_3	0.15	0.24	0.11	0.36	0.09	0.00	0.12	0.05	0.15	0.13	0.17	0.16
Sb_2O_3	0.26	0.18	0.22	0.25	0.00	0.18	0.13	0.08	0.16	0.13	0.20	0.16
SiO_2	0.18	0.19	0.19	0.14	0.29	0.07	0.20	0.22	0.24	0.17	0.22	0.20
As_2O_5	38.09	38.28	37.18	37.38	36.98	38.79	39.41	38.51	41.04	38.13	40.37	39.94
P_2O_5	0.10	0.32	0.10	0.08	0.00	0.00	0.14	0.14	0.17	0.14	0.17	0.16
SO_3	0.38	0.47	0.84	0.81	0.00	0.10	0.11	0.08	0.00	0.18	0.23	0.06
F	0.16	0.11	0.15	0.16	0.19	0.19	0.16	0.16	0.15	0.17	0.14	0.17
H_2O*	11.13	11.43	11.33	11.14	11.08	10.71	12.07	11.87	12.60	11.84	12.34	12.41
O=F	–0.07	–0.05	–0.06	–0.07	–0.08	–0.08	–0.07	–0.07	–0.06	–0.07	–0.06	–0.07
total	106.16	108.05	106.60	105.34	104.23	104.43	112.49	110.41	117.31	109.90	114.93	114.65
Ca^{2+}	0.030	0.033	0.023	0.025	0.074	0.000	0.042	0.042	0.051	0.040	0.041	0.054
Fe^{2+}	0.000	0.000	0.000	0.000	0.000	0.000	0.047	0.033	0.056	0.026	0.100	0.096
Pb^{2+}	0.000	0.000	0.000	0.000	0.000	0.000	0.006	0.000	0.013	0.009	0.004	0.000
Cu^{2+}	8.046	8.033	8.236	8.003	8.340	7.938	8.370	8.462	8.350	8.463	8.194	8.388
Zn^{2+}	0.125	0.163	0.106	0.111	0.176	0.088	0.176	0.197	0.193	0.200	0.174	0.190
Al^{3+}	0.035	0.054	0.025	0.083	0.022	0.000	0.026	0.011	0.032	0.030	0.037	0.035
subtotal	8.236	8.282	8.389	8.222	8.612	8.026	8.668	8.745	8.695	8.768	8.551	8.763
Si^{4+}	0.034	0.036	0.037	0.027	0.059	0.014	0.039	0.043	0.044	0.033	0.041	0.038
Sb^{5+}	0.021	0.014	0.018	0.020	0.000	0.014	0.010	0.006	0.012	0.011	0.015	0.012
As^{5+}	3.874	3.830	3.805	3.820	3.941	3.957	3.913	3.916	3.918	3.906	3.886	3.916
P^{5+}	0.016	0.052	0.017	0.013	0.000	0.000	0.023	0.023	0.026	0.023	0.026	0.025
S^{6+}	0.055	0.068	0.123	0.119	0.000	0.015	0.015	0.012	0.000	0.026	0.032	0.008
subtotal	4.000	4.000	4.000	4.000	4.000	4.000	4.000	4.000	4.000	4.000	4.000	4.000
F^-	0.096	0.067	0.093	0.099	0.122	0.117	0.095	0.098	0.087	0.105	0.082	0.101
OH^-	4.433	4.583	4.798	4.520	5.064	3.936	5.291	5.404	5.348	5.480	5.148	5.526
∑F + OH	4.529	4.649	4.891	4.619	5.186	4.053	5.386	5.502	5.435	5.586	5.230	5.627
H_2O	5.003	5.004	4.998	5.003	5.000	5.002	5.000	4.998	4.999	4.998	5.003	4.999

mean a – mean of all 7 analyses (some not shown here) of fibrous aggregates of strashimirite; 1–5 its selected representative analyses;
mean b – mean of all 11 analyses of strashimirite compact aggregates (6–10 being the selected representative analyses).
Coefficients of empirical formula were obtained assuming (As + P + S + Sb + Si) = 4; H_2O* contents were calculated on the basis of charge balance and theoretical content of five water molecules.

Frost (2000), who reinterpreted the dataset published by Gadsden (1975), the band around 1035 cm^{-1} represents vibration of the CO_3 group or an OH-bend. However, in the case of the high content of sulphate groups, especially in the emerald-green tyrolite, it seems to be more logical to ascribe that band to antisymmetric stretching mode of the SO_4 groups. Interesting is also the band representing symmetric stretching mode of AsO_4 group (808 cm^{-1}), which, for the emerald-green tyrolite, is much lower than in the SO_4-poor, pale blue-green variety. The whole band component analysis for both types of tyrolite from Farbište is presented in Tab. 25.

4.4. Silicates

4.4.1. Chrysocolla

This mineral forms common bluish green to green botryoidal crusts and compact fillings of vugs and fissures in the mineralized rocks. It is mostly associated with tyrolite, malachite, azurite and barite. Common are chrysocolla pseudomorphs after tabular crystals and radial aggregates of tyrolite.

Chrysocolla was identified by semiquantitative microprobe analyses, which show that the main components are

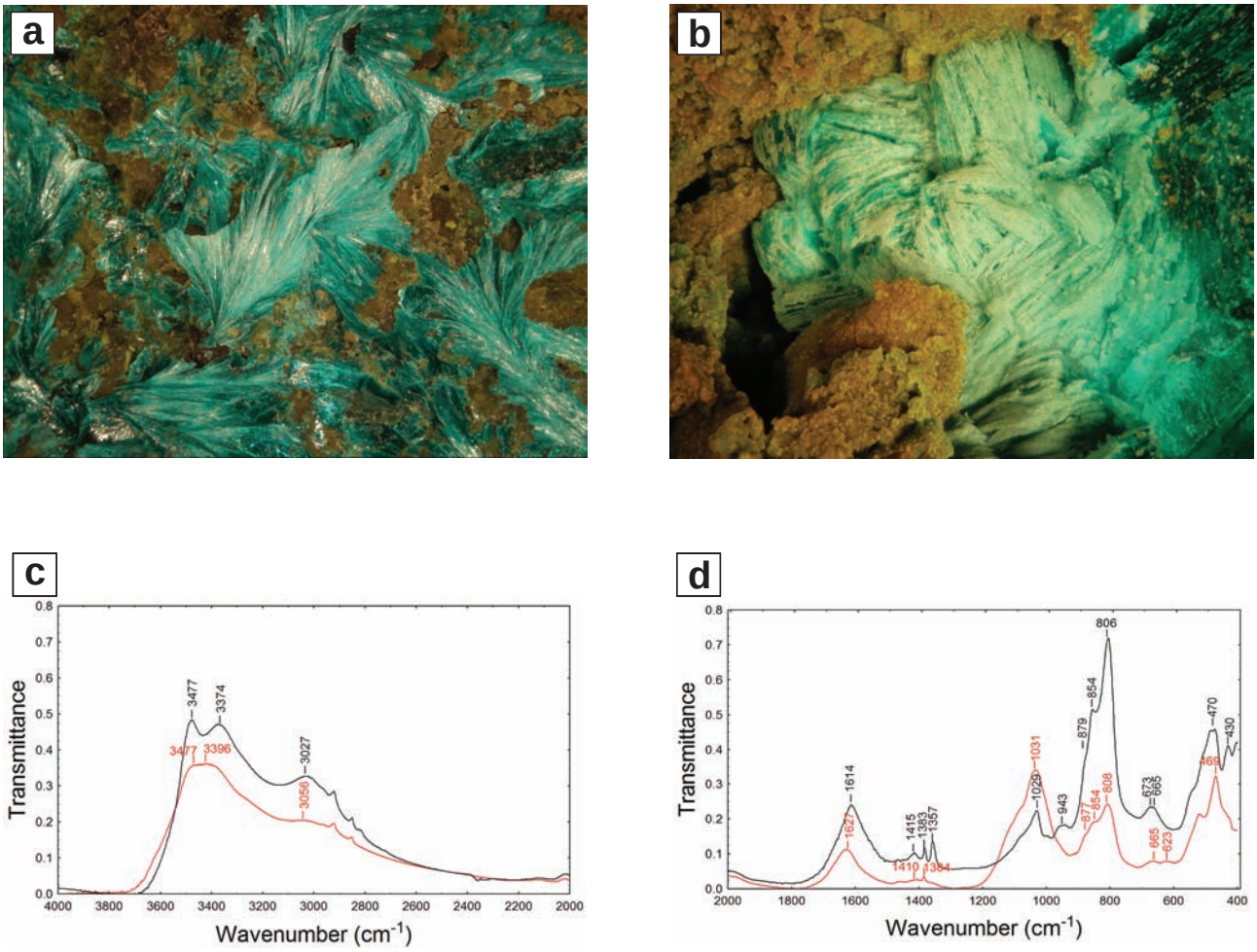

Fig. 15a – Typical radial aggregates of tyrolite. Width of area is 10 mm. Photo by M. Števko. **b** – An irregular aggregate of platy to tabular tyrolite crystals partially replaced by chrysocolla. Width of area is 6 mm. Photo by M. Števko. **c** – Infrared (IR) spectra for both tyrolite types (4000–2000 cm^{-1}): red line (emerald-green tyrolite) and black line (pale blue-green tyrolite). **d** – Infrared (IR) spectra of both tyrolite types (2000–400 cm^{-1}): red line (emerald-green tyrolite) and black line (pale blue-green tyrolite).

Cu, Al, Si and O. According to X-ray powder diffraction, the studied samples are amorphous.

5. Origin and formation of supergene mineralization at the Farbište occurence

Two main associations of the supergene minerals were observed at Farbište occurrence (Fig. 16). Both formed as a result of weathering of primary ore minerals, especially tennantite, which is the dominant primary ore phase and was the main source of Cu, As and S ions in the supergene zone. The almost complete absence of supergene hydroxides and oxides of iron such as goethite is caused by the relative scarcity of pyrite and other iron-bearing minerals in the primary zone.

The first association is typical of the lower part of the supergene zone and is exposed in the upper adit. The main supergene phases in this case are tyrolite and chrysocolla. Relatively common are also barite, azurite and malachite. Except tyrolite, no additional copper arsenates have been observed. The chemical composition of tyrolite from this association is characterised by a predominance of the $(SO_4)^{2-}$ over $(CO_2)^{2-}$ groups in the anion position. This most probably results from the higher activity of Ca^{2+} and $(AsO_4)^{3-}$ ions and the absence of $(CO_3)^{2-}$ in solutions during the early stage of the supergene phases' crystallization sequence. In this situation the $(SO_4)^{2-}$ ions produced by weathering of primary minerals would be preferentially incorporated in tyrolite.

The second association of supergene minerals is represented by a rich suite of copper arsenates and carbonates and is especially well developed in the upper part of the outcrop. Tyrolite is much rarer compared to the previous association. Rare brochantite and mixed-anion sulphate–arsenate species parnauite are

Tab. 22 X-ray powder diffraction pattern of tyrolite

h	*k*	*l*	$d_{obs.}$	I/I_o	$d_{calc.}$	*h*	*k*	*l*	$d_{obs.}$	I/I_o	$d_{calc.}$
1	0	0	26.9	100	26.9	1	0	0	27.2	100	27.3
2	0	0	13.7	25	13.6	2	0	0	13.5	25	13.5
3	0	0	9.06	5	9.09						
0	1	0	5.59	5	5.57	0	1	0	5.54	4	5.53
1	1	0	5.43	5	5.46						
						5	0	0	5.38	4	5.38
1	0	–2	5.24	5	5.23						
						0	0	2	5.19	4	5.21
0	1	1	4.903	5	4.906						
1	1	1	4.781	7	4.774						
						3	0	–2	4.723	5	4.736
2	0	2	4.631	5	4.638						
						2	1	1	4.502	4	4.516
4	0	–2	4.439	6	4.437						
3	1	1	4.198	5	4.203						
5	0	–2	4.049	5	4.051						
						5	0	–2	3.957	5	3.967
4	0	2	3.878	5	3.876						
						4	1	1	3.855	4	3.859
1	–1	–2	3.811	5	3.813	1	–1	–2	3.803	4	3.796
3	–1	–2	3.631	4	3.637						
4	–1	–2	3.472	5	3.470						
3	1	2	3.387	5	3.382						
						8	0	0	3.374	5	3.364
7	1	1	2.954	6	2.958						
						1	–1	–3	2.952	6	2.953
3	–1	–3	2.899	5	2.897						
						8	0	2	2.694	5	2.695
0	2	1	2.687	5	2.689						
3	2	0	2.662	5	2.662						
						1	–2	–1	2.662	6	2.666
3	–2	–1	2.609	4	2.604						
						0	0	4	2.602	4	2.605
4	2	0	2.576	4	2.578	4	2	0	2.559	4	2.556
1	0	4	2.549	4	2.549						
						4	–2	–1	2.507	4	2.507
4	2	1	2.473	4	2.471						
						5	0	–4	2.4520	5	2.4524
2	–1	–4	2.3651	4	2.3674						
						6	2	0	2.3514	4	2.3530
2	2	3	2.1198	3	2.1132						
						3	2	3	2.0729	3	2.0704
1	–2	–4	1.9092	3	1.9066						
1	3	0	1.8515	3	1.8518						
						5	3	0	1.7427	3	1.7432
						3	3	2	1.6905	3	1.6939

Tab. 23 Unit-cell parameters of tyrolite (for monoclinic space group $P2_1/c$)

Occurrence	**Reference**	***a* [Å]**	***b* [Å]**	***c* [Å]**	***β*°**	***V* [Å³]**
Farbište, Slovakia	this paper (emerald green)	27.078(5)	5.5275(7)	10.4817(12)	96.293(14)	1559.3(3)
Farbište, Slovakia	this paper (pale blue green)	27.543(3)	5.5681(6)	10.4763(9)	98.009(9)	1591.02(3)
Brixlegg, Tyrol, Austria	Krivovichev et al. (2006) – polytype 1*M*	27.562(3)	5.5682(7)	10.4662(15)	98.074(11)	1590.3(3)
Brixlegg, Tyrol, Austria	Krivovichev et al. (2006) – polytype 2*M*	54.520(6)	5.5638(6)	10.4647(10)	96.432(9)	3154.4(6)

Tab. 24 Chemical composition of tyrolite (in wt. %)

	mean 1–3	1	2	3	mean 4–7	4	5	6	7
CaO	7.01	6.89	6.95	7.18	7.27	7.20	7.28	7.30	7.31
PbO	0.07	0.00	0.13	0.09	0.06	0.14	0.00	0.09	0.00
CuO	44.91	44.56	45.15	45.01	45.94	45.68	46.80	45.42	45.84
ZnO	0.16	0.11	0.23	0.13	0.15	0.22	0.10	0.16	0.13
As_2O_5	29.99	29.80	30.14	30.02	30.31	30.59	30.42	29.43	30.78
P_2O_5	0.43	0.43	0.41	0.46	0.42	0.39	0.44	0.44	0.41
SO_3	1.32	1.26	1.08	1.63	0.29	0.21	0.24	0.48	0.24
F	0.12	0.12	0.14	0.11	0.12	0.17	0.12	0.11	0.09
CO_2*	0.33	0.23	0.50	0.27	1.39	1.06	1.72	1.84	0.93
H_2O*	17.98	17.87	18.04	18.04	18.16	18.28	18.25	17.67	18.44
O=F	–0.05	–0.05	–0.06	–0.05	–0.05	–0.07	–0.05	–0.05	–0.04
total	102.27	101.22	102.71	102.89	104.06	103.87	105.32	102.89	104.13
Ca^{2+}	1.872	1.852	1.849	1.913	1.924	1.890	1.917	1.985	1.906
Pb^{2+}	0.005	0.000	0.009	0.006	0.004	0.009	0.000	0.006	0.000
ΣCa + Pb	1.876	1.852	1.858	1.919	1.928	1.900	1.917	1.991	1.906
Cu^{2+}	8.456	8.444	8.470	8.455	8.567	8.455	8.687	8.708	8.425
Zn^{2+}	0.029	0.020	0.042	0.024	0.028	0.040	0.018	0.030	0.023
ΣCu + Zn	8.485	8.464	8.512	8.479	8.595	8.495	8.705	8.738	8.448
As^{5+}	3.909	3.909	3.914	3.903	3.912	3.919	3.908	3.905	3.916
P^{5+}	0.091	0.091	0.086	0.097	0.088	0.081	0.092	0.095	0.084
ΣAs + P	4.000	4.000	4.000	4.000	4.000	4.000	4.000	4.000	4.000
S^{6+}	0.248	0.237	0.201	0.304	0.054	0.039	0.044	0.091	0.044
C^{4+}	0.112	0.079	0.170	0.092	0.469	0.355	0.577	0.638	0.309
ΣS + C	0.360	0.316	0.371	0.396	0.523	0.393	0.621	0.729	0.353
F^-	0.097	0.095	0.110	0.087	0.096	0.132	0.093	0.088	0.069
OH^-	7.906	7.905	7.889	7.917	7.904	7.870	7.908	7.912	7.932
ΣOH + F	8.003	8.000	7.999	8.003	8.000	8.002	8.001	8.000	8.002
H_2O	10.997	10.999	10.999	11.004	11.003	11.004	11.004	11.002	10.997

Means and representative analyses of tyrolite from Farbište. 1–3: emerald-green platy crystals; 4–6: pale blue-green radial aggregates. Coefficients of empirical formula were obtained assuming (As + P) = 4; CO_2* and H_2O* were calculated on the basis of ideal contents (OH + F) = 8, H_2O = 11 and charge balance.

Tab. 25 Band component analysis of the infrared spectrum of both tyrolite types

emerald green crystals		pale blue-green aggregates		tentative assignment
[cm^{-1}]		[cm^{-1}]		
3477	0.356	3477	0.583	ν O–H stretch (hydroxyl ions)
3396	0.358	3375	0.571	ν O–H stretch (molecular water, hydroxyl ions)
3057	0.205	3028	0.428	ν O–H stretch (molecular water)
1628	0.112	1614	0.341	δ H_2O bend
		1416	0.203	ν_3 CO_3 antisymmetric stretch
1385	0.038	1383	0.218	ν_3 CO_3 antisymmetric stretch
		1358	0.236	ν_3 CO_3 antisymmetric stretch
1032	0.341	1030	0.324	ν_3 SO_4 antisymmetric stretch
		943	0.282	δ M–OH bend, H_2O libration (?)
877	0.155	879	0.467	ν_3 AsO_4 antisymmetric stretch/ν_2 CO_3 bend (?)
854	0.189	854	0.616	ν_3 AsO_4 antisymmetric stretch
808	0.243	806	0.819	ν_1 AsO_4 symmetric stretch
673	0.079	673	0.335	ν_4 CO_3 bend
665	0.080	665	0.335	ν_4 CO_3 bend
642	0.076			ν_4 SO_4 bend
623	0.079			ν_4 SO_4 bend
469	0.324	471	0.558	ν_4 AsO_4 bend
		430	0.510	ν_4 AsO_4 bend

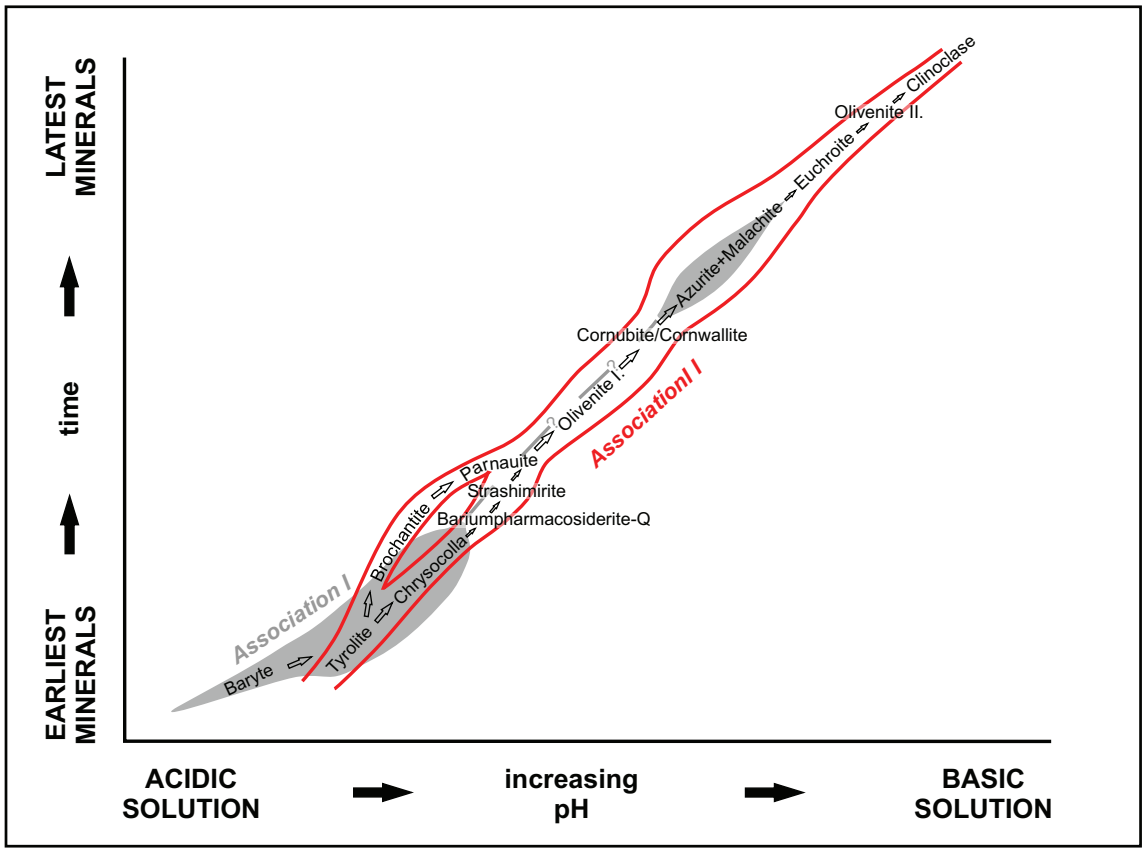

Fig. 16 Inferred crystallization sequence of supergene minerals at Farbište ore occurrence.

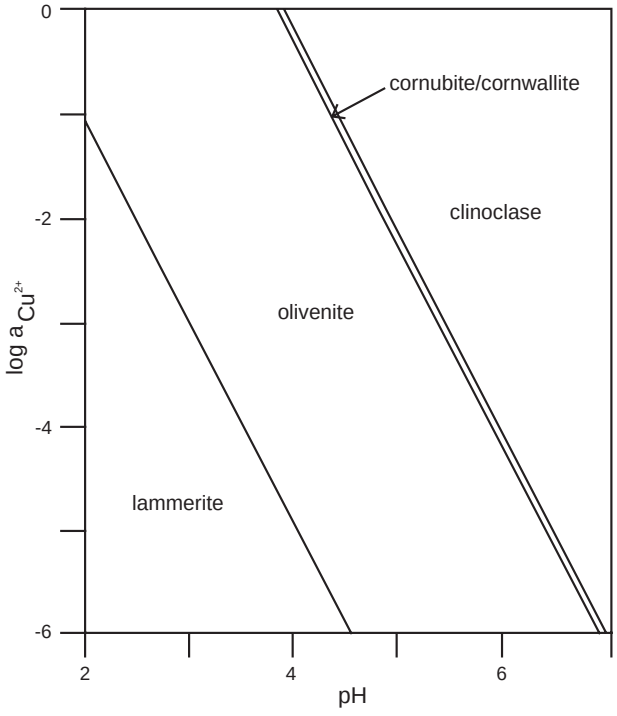

Fig. 17 Stability field diagram for the supergene Cu(II) arsenate minerals (Magalhães et al. 1988).

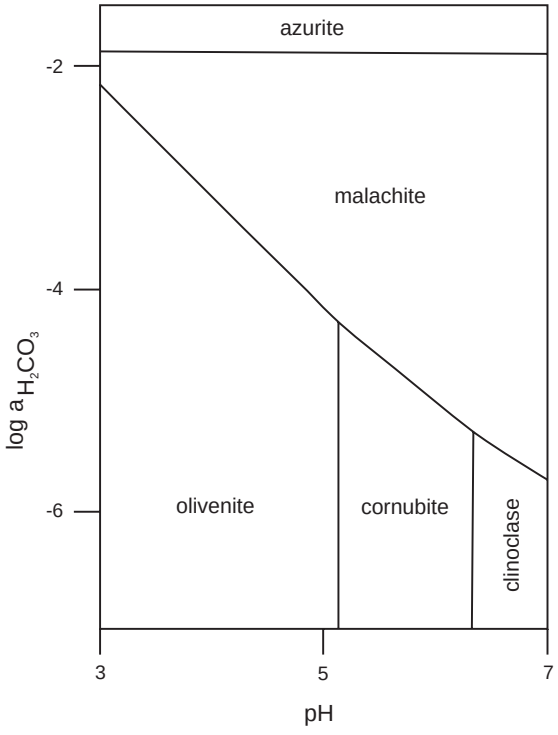

Fig. 18 Boundaries between the copper (II) arsenates and more common supergene carbonate minerals (Magalhães et al. 1988).

also present together with tyrolite. This fact is well reflected in the chemical composition of tyrolite, which contains $(CO_3)^{2-}$ groups predominating over $(SO_4)^{2-}$ in the interlayer positions, because most of the $(SO_4)^{2-}$ is bound in brochantite and parnauite. Due to the isolated nature of the brochantite occurrence, it is difficult to define its exact relation to other copper arsenates in the sequence. However, the position of brochantite as one of the oldest supergene phases is confirmed by the fact that is replaced by parnauite. Parnauite was observed elsewhere as crusts on strashimirite. Both brochantite and parnauite are covered by azurite and malachite. The presence of bariopharmacosiderite-Q as an earlier phase in the crystallization sequence indicates a rapid decline in activity of Fe^{3+} ions in the solution during the crystallization of supergene minerals.

According to data published by Magalhães et al. (1988) and Williams (1990), olivenite is a stable phase at relatively lower, and clinoclase at higher, pH conditions (Fig. 17). Cornubite (or cornwallite) is stable only in the very narrow field between olivenite and clinoclase. In general, more basic stoichiometries occupy fields at higher pH values (Magalhães et al. 1988). Thus, the observed broad crystallization sequence of copper arsenates at Farbište – tyrolite → strashimirite → olivenite I → cornubite + cornwallite → euchroite → olivenite II → clinoclase – obviously represents a slight increase in the pH values and/or copper ion activity in the solution. Numerous associations with clinoclase covering olivenite or cornubite/cornwallite are known (e.g. Řídkošil 1981b; Embrey and Symes 1987; Wendel et al. 2001; Dunning and Cooper 2005; Szakáll et al. 2005). A reverse paragenetic sequence of copper arsenates was described from the Majuba Hill mine, Nevada, where clinoclase crystallized first and was followed by cornwallite, cornubite and olivenite (Jensen 1985). A similar association was reported also from the Dome Rock copper mine, South Australia (Ryall and Segnit 1976) and the Gelnica copper deposit in Slovakia (Sejkora et al. 2001). Such a sequence reflects presumably a drop in pH values and/or Cu^{2+} activity during crystallization (Magalhães et al. 1988). Solution studies of copper arsenates revealed that strashimirite and also euchroite are metastable phases with respect to olivenite (Magalhães et al. 1988). According to Guillemin (1956), natural or synthetic euchroite is transformed to olivenite in aqueous solution at pH ~ 5.4 and elevated temperatures. Euhedral olivenite inclusions are characteristic of euchroite from Farbište, especially of opaque crystals. Rarely, also complete pseudomorphs of olivenite after euchroite were observed. A similar situation (euhedral olivenite inclusions) is also known from the type locality of euchroite, the Svätodušná deposit near Ľubietová, Slovakia (Figuschová 1977). Such olivenite inclusions enclosed in euchroite or olivenite pseudomorphs after the latter mineral represent most probably a product of a partial decomposition of the euchroite as metastable phase. The position of azurite and malachite among copper arsenates in the crystallization sequence indicates a local increase in activity of CO_2 (Fig. 18), the exact cause of which remains unknown. According to Williams (1990), azurite is the stable carbonate phase at the elevated activity of CO_2. The fact that the studied azurite is clearly older than the malachite could indicate a decreasing CO_2 activity during that stage of the supergene zone evolution.

Acknowledgements. The authors wish to thank Peter Tuček, Michal Krupa and Tomáš Bancík who kindly provided some samples for study, Radek Škoda (Masaryk University, Brno) and Stanislav Vrána (Czech Geological Survey, Prague) for their support of this study and Volker Betz for excellent photos of few studied specimens. Both referees, William D. Birch and Stuart J. Mills, same as handling editor Jakub Plášil and the editor-in-chief Vojtěch Janoušek, are highly acknowledged for comments and suggestions that helped to improve the manuscript. This work was financially supported by the Ministry of Culture of the Czech Republic (MK00002327201) to JS as well as by the Comenius University research grant UK/50/2011 and by the Slovak Research and Development Agency under the contract No. APVV-VVCE-0033-07 SOLIPHA to MŠ and PB.

References

Anthony JW, Bideaux RA, Bladh KW, Nichols MC (2000) Handbook of Mineralogy. Volume IV – Arsenates, Phosphates, Vanadates. Mineral Data Publishing, Tucson, pp 1–680

Arlt T, Armbruster T (1999) Single-crystal X-ray structure refinement of cornwallite, $Cu_5(AsO_4)_2(OH)_4$: a comparison with its polymorph cornubite and the PO_4 analogue pseudomalachite. Neu Jb Mineral, Mh 10: 468–480

Burns PC, Hawthorne FC (1995) Rietveld refinement of the crystal structure of olivenite: a twinned monoclinic structure. Canad Mineral 33: 885–888

Bystrický J (1964) Stratigraphy and evolution of Drienok series. Zpr geol Výsk v roku 1963 2: 94–96 (in Slovak)

Čech V, Fediuková E, Kotrba Z, Táborský Z (1975) Occurrence of barium-pharmacosiderite in tourmalinite from southern Bohemia. Čas Mineral Geol 20: 423–425 (in Czech)

Dunning GE, Cooper JF (2005) Mineralogy of the Spring Creek area, Last Chance mining district, Plumas County, California. Axis 1: 1–30

Eby RK, Hawthorne FC (1989) Euchroite, a heteropolyhedral framework structure. Acta Cryst C45: 1479–1482

Eby RK, Hawthorne FC (1990) Clinoclase and the geometry of 5-coordinate Cu^{2+} in minerals. Acta Cryst C46: 2291–2294

Embrey PG, Symes RF (1987) Minerals of Cornwall and Devon. British Museum (Natural History), London, pp 1–154

Figuschová M (1977) Supergene copper minerals from Ľubietová. In: Zborník z konferencie Ložiskotvorné procesy Západných Karpát. Prírodovedecká fakulta Univerzity Komenského, Bratislava, 135–137 (in Slovak)

Frost RL, Sejkora J, Čejka J, Keeffe EC (2009a) Raman spectroscopic study of the mixed anion sulphate–arsenate mineral parnauite $Cu_9[(OH)_{10}|SO_4|(AsO_4)_2]\cdot 7H_2O$. J Raman Spectrosc 40: 1546–1550

Frost RL, Sejkora J, Čejka J, Keeffe EC (2009b) Vibrational spectroscopic study of the arsenate mineral strashimirite $Cu_8(AsO_4)_4(OH)_4\cdot 5H_2O$ – relationship to other basic copper arsenates. Vibrat Spectrosc 50: 289–297

Frost RL, Čejka J, Sejkora J, Plášil J, Bahfenne S, Palmer SJ (2010) Raman spectroscopy of the basic copper arsenate mineral: euchroite. J Raman Spectrosc 41: 571–575

Gadsden JA (1975) Infrared Spectra of Minerals and Related Inorganic Compounds. Butterworth & Co. Publisher Ltd., London, pp 1–96

Gołębiowska B (1999) Strashimirite and cornwallite (copper arsenates) from Rędziny (Lower Silesia, Poland). Mineral Polonica 30: 3–11

Guillemin C (1956) Contribution a la Mineralogie des arséniates, phosphates et vanadates de cuivre. Bull Soc franç Minéral Cristallogr 79: 7–95

Hager SL, Leverett P, Williams PA, Mills SJ, Hibbs DE, Raudsepp M, Kampf AR, Birch WD (2010) The single-crystal X-ray structures of bariopharmacosiderite-*C*, bariopharmacosiderite-*Q* and natropharmacosiderite. Canad Mineral 48: 1477–1485

Helliwell M, Smith JV (1997) Brochantite. Acta Cryst C53: 1369–1371

Hyršl J, Korbel P, Šourek J (1984) Cornubite and cornwallite from Farbište near Ponická Lehôtka. Čas Mineral Geol 29: 433–434 (in Czech)

Jansa J, Novák F, Pauliš P, Schramová M (1998) Supergene minerals of the Sn–W deposit Cínovec, the Krušné hory Mountains (Czech Republic). Bull mineral-petrolog Odd Nár Muz (Praha) 6: 83–101 (in Czech)

Jensen M (1985) The Majuba Hill Mine, Pershing County, Nevada. Min Record 16: 57–72

Kloprogge JT, Frost RL (2000) A Raman microscopy study of tyrolite, a multi-anion arsenate mineral. App Spectrosc 54: 517–521

Kotásek J, Kuděsásek V (1962) Notes on the metallogeny and geology of the southwestern part of Veporic Unit. Geol Práce, Zprávy 25–26: 105–134 (in Czech with German summary)

Kravjanský I (1962) Notes on ore mineralization in the Nízke Tatry Mts. and adjacent mountains. Geol Práce, Zošit 62: 155–164 (in Slovak)

Krivovichev SV, Chernyshov DY, Döbelin N, Armbruster T, Kahlenberg V, Kaindl R, Ferraris G, Tessadri R, Kaltenhauser G (2006) Crystal chemistry and polytypism of tyrolite. Amer Miner 91: 1378–1384

Láznička P (1965) Regional mineralogical situation in the Central Slovakia. Národní Muzeum, Prague, pp 1–35 (in Czech)

Li CH, Yang H, Downs RT (2008) Redetermination of olivenite from an untwined single-crystal. Acta Cryst E64: i60–i61

Losert J. (1965) Ore deposits in the western part of the Ľubietová Zone and adjacent Subtatricum. Sbor Geol Věd, Ložisk Geol Mineral 6: 7–39 (in Czech)

Ma Z, Qian R, Peng Z (1980) Clinotyrolite: a new mineral of the hydrous copper arsenate discovered in Dongchuan, Yunnan. Acta Geol Sin 54: 134–143 (in Chinese with English abstract)

Magalhães MCF, Pedrosa de Jesus JD, Willians PA (1986) Stability constants and formation of Cu(II) and Zn(II) phosphate minerals in the oxidized zone of base metal orebodies. Mineral Mag 50: 33–39

Magalhães MCF, Pedrosa de Jesus JD, Willians PA (1988) The chemistry of formation of some secondary arsenate minerals of Cu(II), Zn(II) and Pb(II). Mineral Mag 52: 679–690

Mazúr E, Lukniš M (1980) Geomorphological Units. In: Mazúr E (ed) Atlas SSR. Veda, Bratislava, pp 1–88 (in Slovak)

Merlino S, Perchiazzi N, Franco D (2003) Brochantite, $Cu_4SO_4(OH)_6$: OD character, polytypism and crystal structures. Eur J Mineral 15: 267–275

Minčeva-Stefanova J (1968) Strashimirite – new hydrated copper arsenate. Zap Vses Mineral Obsch 97: 470–477 (in Russian)

Minčeva-Stefanova J (1998) Strashimirite from the Venetsa deposit, Western Balkan Mountain as an informator about its morphological diversity and two types of parageneses. Geochem Mineral and Petrol 33: 3–14

Mutter G, Eysel W, Greis I, Schmetzer K (1984) Crystal chemistry of natural and ion-exchanged pharmacosiderites. Neu Jb Mineral, Mh 183–192

Ondruš P, Veselovský F, Hloušek J, Skála R, Vavřín I, Frýda J, Čejka J, Gabašová A (1997) Secondary minerals of the Jáchymov (Joachimsthal) ore district. J Czech Geol Soc 42: 3–69

Peacor DR, Dunn PJ (1985) Sodium-pharmacosiderite, a new analog of pharmacosiderite from Australia and new occurrences of barium-pharmacosiderite. Mineral Record 16: 121–124

Polák M, Filo I, Havrila M, Bezák V, Kohút M, Kováč P, Vozár J, Mello J, Maglay J, Elečko M, Vozárová A, Olšavský M, Siman P, Buček S, Siráňová Z, Hók J,

Rakús M, Lexa J, Šimon L, Pristaš J, Kubeš P, Zakovič M, Liščák P, Žáková E, Boorová D, Vaněková H (2003a) Geological map of the Starohorské vrchy Mts., Čierťaž Mts. and northern part of the Zvolenská kotlina depression, 1:50 000. Slovak Geological Survey, Bratislava

Polák M, Filo I, Havrila M, Bezák V, Kohút M, Kováč P, Vozár J, Mello J, Maglay J, Elečko M, Vozárová A, Olšavský M, Siman P, Buček S, Siráňová Z, Hók J, Rakús M, Lexa J, Šimon L, Pristaš J, Kubeš P, Zakovič M, Liščák P, Žáková E, Boorová D, Vaněková H (2003b) Outline of geological structure of the Starohorské vrchy Mts., Čierťaž Mts. and northern part of the Zvolenská kotlina depression, 1:50 000. Slovak Geological Survey, Bratislava, pp 1–218 (in Slovak)

Pouchou JL, Pichoir F (1985) "PAP" (φρZ) procedure for improved quantitative microanalysis. In: Armstrong JT (ed) Microbeam Analysis. San Francisco Press, San Francisco, pp 104–106

Putiš M, Kotov AB, Uher P, Salnikova EB, Korikovsky SP (2000) Triassic age of the Hrončok pre-orogenic A-type granite related to continental rifting: a new result of U–Pb isotope dating (Western Carpathians). Geol Carpath 51: 59–61

Ryall WR, Segnit ER (1976) Minerals of oxidized zone of the Dome Rock copper deposit, South Australia. Austral Min 2: 5–8

Řídkošil T (1978) Novoveská Huta – new occurrence of rare supergene copper minerals. Čas Miner Geol 23: 214–215 (in Czech)

Řídkošil T (1981a) Arsenates of copper from Farbište in the central Slovakia. Čas Mineral Geol 26: 92 (in Czech)

Řídkošil T (1981b) Clinoclase from Novoveská Huta, Slovakia. Acta Univ Carol, Geol 1: 45–52 (in Czech with English and Russian summaries)

Sato E, Nazai I, Terada Y, Tsutsumi Y, Yokoyama K, Miawaki R, Matsubara S (2008) Study of Zn-bearing beaverite $Pb(Fe_2Zn)(SO_4)_2(OH)_6$ obtained from Mikawa mine, Niigata Prefecture, Japan. Jour Mineral Petrol Sci 103: 141–144

Sejkora J, Ďuďa R, Novotná M (2001) Minerals of oxide zone of the Krížová vein, Gelnica, the Slovenské Rudohorie Mts., Slovak Republic. Bull mineral-petrolog Odd Nár Muz (Praha) 9: 121–139 (in Czech)

Sejkora J, Ondruš P, Fikar M, Veselovský F, Mach Z, Gabašová A, Škoda R, Beran P (2006) Supergene minerals at the Huber stock and Schnöd stock deposits, Krásno ore district, the Slavkovský les area, Czech Republic. J Czech Geol Soc 51: 57–101

Sejkora J, Škovíra J, Čejka J, Plášil J (2009) Cu-rich members of the beudantite–segnitite series from the Krupka ore district, the Krušné hory Mountains, Czech Republic. J Geosci 54: 355–371

Slavkay M (1965) Mesozoic volcanogenic rocks in the vicinity of Poniky. Čas Mineral Geol 10: 249–259 (in Slovak with English summary)

Slavkay M (1971) Polymetallic ore deposits near Poniky. Miner Slov 3: 181–213 (in Slovak with French and English summaries)

Slavkay M, Tomko I, Lukaj M, Barkaj Z (1968) Poniky, Pb Ores, Final Report and Calculation of Reserves. Unpublished manuscript, Slovak Geological Survey, Bratislava, pp 1–387 (in Slovak)

Szakáll S, Gatter I, Szendrei G (2005) Hungarian Minerals. Kőország Kiadó, Budapest, pp 1–427 (in Hungarian)

Števko M, Bálintová T, Turecký L (2010) Euchroit-Neufunde und seltene Kupfermineralien aus Farbište bei Poniky, Slowakei. Lapis 35: 25–29

Tillmanns E, Hofmeister W, Petitjean K (1985) Cornubite, $Cu_5(AsO_4)_2(OH)_4$, first occurrence of single crystals, mineralogical description and crystal structure. Bull Geol Soc Finland 57: 119–127

Uher P, Ondrejka M, Spišiak J, Broska I, Putiš M (2002) Lower Triassic potassium-rich rhyolites of the Silicic Unit, Western Carpathians, Slovakia: geochemistry, mineralogy and genetic aspects. Geol Carpath 53: 27–36

Vozárová A, Vozár J (1988) Late Paleozoic in Western Carpathians. Slovak Geological Survey, Bratislava, pp 1–314

Wendel W, Bayerl R, Oppelt W (2001) Mineralien der Grube Clara bei Oberwolfach. Lapis 26: 27–54

Williams PA (1990) Oxide Zone Geochemistry. Ellis Horwood Ltd., Chichester, pp 1–286

Wise WS (1978) Parnauite and goudeyite, two new copper arsenate minerals from the Majuba Hill mine, Pershing County, Nevada. Amer Miner 63: 704–708

Zepharovich V (1859) Mineralogisches Lexikon für das Kaisertum Österreich. Band I. Wilhelm Braumüller, Wien, pp 1–627

Zipser CHA (1817) Versuch eines topographisch–mineralogischen Handbuches von Ungern. Carl Friedrich Wigand, Oedenburg, pp 1–440